Received XX Month, XXXX; revised XX Month, XXXX; accepted XX Month, XXXX; Date of publication XX Month, XXXX; date of current version XX Month, XXXX.

Digital Object Identifier 10.1109/XXXX.2022.1234567

Sparse DOA Estimation with Polarimetric Arrays

Augusto Aubry[1], Senior Member, IEEE, Marco Boddi[1], Antonio De Maio[1], Fellow, IEEE, and Massimo Rosamilia[1], Member, IEEE

[1]Department of Electrical Engineering and Information Technology, Università degli Studi di Napoli "Federico II", DIETI, Via Claudio 21, I-80125 Napoli, Italy

Corresponding author: A. De Maio (email: ademaio@unina.it).

The work of A. Aubry, A. De Maio, and M. Rosamilia was partially supported by the European Union under the Italian National Recovery and Resilience Plan (NRRP) of NextGenerationEU, partnership on "Telecommunications of the Future" (PE00000001 - program "RESTART").

ABSTRACT This paper addresses the Direction-of-Arrival (DOA) estimation problem using a narrowband polarimetric array sensing system. The considered receiving equipment is composed of two sub-arrays of sensors with orthogonal polarizations. By suitably modeling the received signal via a sparse representation (accounting for the multiple snapshots and the polarimetric array manifold structure), two iterative algorithms, namely Polarimetric Sparse Learning via Iterative Minimization (POL-SLIM) and Polarimetric Sparse Iterative Covariance-based Estimation (POL-SPICE), are devised to accomplish the estimation task. The proposed algorithms provide accurate DOA estimates while enjoying nice (rigorously proven) convergence properties. Numerical analysis shows the effectiveness of POL-SLIM and POL-SPICE to successfully locate signal sources in both passive sensing applications (with large numbers of collected snapshots) and radar spatial processing, also in comparison with single-polarization counterparts as well as theoretical benchmarks.

INDEX TERMS DOA estimation, polarimetry, sparse methods, high resolution

I. INTRODUCTION

DIRECTION-of-Arrival (DOA) estimation holds a paramount significance across diverse domains encompassing radar systems, wireless communications, and sonar signal processing [1]–[3]. The accurate localization of incident signals is crucial for beamforming, source positioning, and interference cancellation applications [4], [5]. Over the past decades, a plethora of algorithms have been proposed to accomplish the DOA estimation task, fulfilling constantly increasing requirements, including high resolution, robustness to sources' correlation, and low computational demands. In this regard, the estimation strategies can be classified into spectral-based, parametric, and compressed sensing methods.

Spectral-based techniques, like beamforming-based and subspace-based methods, exploit the measurements of an appropriate spatial spectrum, identifying spectral peaks to obtain corresponding DOA estimates. The Conventional Beamformer (CBF) is a standard technique to maximize the output power in a specific direction where the signal of interest is presumed to be present. However, it has limited angular resolution and high sidelobes. To overcome its limitations, different beamformers, like Capon Minimum Variance Distortionless Response (MVDR), have been proposed [6], albeit with operative limitations in high Signal-to-Noise Ratio (SNR) scenarios, when the sample covariance matrix can be ill-conditioned.

Subspace-based super-resolution methods, such as MUltiple SIgnal Classification (MUSIC) and Estimation of Signal Parameters Via Rotational Invariance Techniques (ESPRIT), are computationally and statistically efficient (under some technical conditions [3]) algorithms based on the covariance matrix eigenvalue decomposition. While the MUSIC algorithm utilizes the noise subspace in the estimation process, ESPRIT leverages the rotational invariance property of specific subarrays, i.e., it calculates the eigenvalues of a matrix that relates two signal subspaces [5], [7]. However, this kind of methods experience severe performance degradation in the presence of correlated or coherent sources (for instance when some forms of signal multipath are present), i.e., when the signal subspace becomes rank deficient [8]–[10]. Two well-known strategies to address this issue are Forward-Backward (FB) averaging and spatial smoothing [3], [11].

Different approaches to tackle the DOA estimation problem include parametric methods like Maximum Likelihood (ML) [3]. In this regard, by considering different hypotheses about the waveform model of the source signals, two estimators have been proposed in the open literature, i.e., Stochastic Maximum Likelihood (SML) and Deterministic Maximum Likelihood (DML) [12], [13]. In the former case, source signals are modeled as Gaussian processes, while in the latter, they are considered as unknown deterministic quantities. Noteworthy algorithms in this context include Iterative Quadratic ML (IQML) [3], [14] and Root-Weighting Subspace Fitting (WSF) [15].

Recently, sparse methods have gained significant attention in the signal processing community due to their ability to yield high-resolution and reliable estimates from a limited number of noisy observations, as well as the capability to handle coherent and correlated sources [16], [17]. They exploit the inherent sparsity of the signal model, where only a few sources contribute to the observed data. Therefore, under the assumption that the DOAs of the sources lie on the assumed dictionary grid, they can be actually retrieved as the support of the sparse signal [18]. In this context, hyperparameter-free algorithms are Sparse Learning via Iterative Minimization (SLIM) [19], [20] and Sparse Iterative Covariance-based Estimation (SPICE) [21] [18], [22]. The former is a regularized minimization algorithm capable of providing accurate signal parameters estimates with a relatively low computational burden [19]. Assuming Gaussian and uncorrelated sources (although it is practically robust to these assumptions), the latter relies on a a covariance fitting criterion with global convergence properties [21] (see also [18] and references therein).

On a parallel track, several promising approaches involved the joint exploitation of both spatial and polarization domains to boost the DOA estimation performance. In fact, by leveraging the spatial information captured by multiple antennas and the polarization characteristics of the incident waves, enhanced accuracy and reliability of the DOA estimates can be obtained [23]–[27]. As a matter of fact, it is well known that diversely polarized arrays are capable of providing better estimation accuracy than the corresponding single polarized arrays [25], [28]–[30]. However, in the open literature, the investigation of sparse estimation techniques leveraging the polarimetric domain to provide high resolution and robust DOA estimates has only received a limited attention. To fill this gap, in this paper, the polarimetric version of [19] and [21], referred to as Polarimetric SLIM (POL-SLIM) and Polarimetric SPICE (POL-SPICE), respectively, are introduced for DOA estimation in a polarimetric sensor array equipped with receive pairs of elements with orthogonal polarizations (for instance, pairs of crossed dipoles).

The main contributions of the present work can be summarized as follows[1]:

1) the formulation of a sparse signal model accounting for both polarizations and spatial characteristics of the emitters;
2) the derivation of POL-SLIM and POL-SPICE algorithms that capitalize on the sparsity of the signal model to endow improved performance to the DOA estimation process, which represents the main novelty of this paper;
3) the study of the convergence properties for the devised procedures in terms of achieving a stationary point of the corresponding optimization problem;
4) an extensive numerical analysis including a passive sensing scenario as well as a radar setup where the active system operates in the presence of vertical multipath. To highlight the effectiveness of the devised estimators, the results are compared with the single-polarization counterparts already available in the open literature and the Cramér-Rao Bound (CRB).

The remainder of this paper is organized as follows. Section II presents the polarimetric signal model. In Section III, the DOA estimation problem is introduced and the proposed POL-SLIM and POL-SPICE solution strategies are discussed. Section IV addresses the performance analysis. Finally, Section V concludes the paper and highlights potential future research directions.

A. NOTATIONS

Boldface is used for vectors $\boldsymbol{a}$ (lower case), and matrices $\boldsymbol{A}$ (upper case). $\boldsymbol{I}_N$ and $\boldsymbol{0}$ denote respectively the $N \times N$ identity matrix and the matrix with zero entries (its size is determined from the context). The notation $\boldsymbol{A}(m)$ is used to represent the $m-th$ column of the matrix $\boldsymbol{A}$. The transpose, conjugate, and conjugate transpose operators are denoted by the symbols $(\cdot)^{\mathrm{T}}$, $(\cdot)^{\star}$, and $(\cdot)^{\dagger}$, respectively. The trace of the matrix $\boldsymbol{A} \in \mathbb{C}^{N \times N}$ is indicated with $\mathrm{tr}(\boldsymbol{A})$. The Kronecker and the Hadamard (element-wise) products are denoted by $\otimes$ and $\odot$, respectively. $\mathbb{R}^N$ and $\mathbb{C}^N$ are respectively the sets of N-dimensional column vectors of real and complex numbers. The letter j represents the imaginary unit (i.e., $j = \sqrt{-1}$). For any complex number x, $\mathfrak{Re}(x)$, $\mathfrak{Im}(x)$, and $|x|$ are used to denote the real part, imaginary part, and the modulus of x, respectively. $\lambda_{\max}(\boldsymbol{A})$ and $\lambda_{\min}(\boldsymbol{A})$ are the maximum and the minimum eigenvalue of $\boldsymbol{A}$, respectively. For any $\boldsymbol{x} \in \mathbb{C}^N$, $\|\boldsymbol{x}\|$ represents the Euclidean norm. Moreover, for any $\boldsymbol{A} \in \mathbb{C}^{N \times N}$, $\|\boldsymbol{A}\|_F$ denotes the Frobenius norm of $\boldsymbol{A}$. Let $\boldsymbol{A}$, $\boldsymbol{B}$ be two square matrices of arbitrary size, $\mathrm{diag}(\boldsymbol{A}, \boldsymbol{B})$ represents the block diagonal matrix with blocks $\boldsymbol{A}$ and $\boldsymbol{B}$. Finally, let $\mathcal{Z}$ be a generic finite set, $\#\{\mathcal{Z}\}$ returns its cardinality.

II. SIGNAL MODEL

Let us consider a sensor array equipped with N receive pairs of crossed-dipoles (elements with orthogonal polarizations which are referred to as horizontal and vertical from now on), collecting data in the presence of K narrowband Ra-

[1]Part of this paper has been presented at the 2023 IEEE International Workshop on Technologies for Defense and Security (TechDefense) [31].

dio Frequency (RF) emitters and aimed at estimating their azimuth angle. The source signals impinge on the array from unknown angular directions $\bar{\theta}_1, \ldots, \bar{\theta}_K$. The baseband discrete-time signal at the output of the receiving array for the l-th snapshot, $l = 1, \ldots, L$, can be modeled as [20]

$$\boldsymbol{y}_l = \left[\boldsymbol{y}_l^{(\mathrm{H})\mathrm{T}}, \boldsymbol{y}_l^{(\mathrm{V})\mathrm{T}}\right]^{\mathrm{T}} = \sum_{m=1}^{K} \boldsymbol{S}(\bar{\theta}_m)\bar{\boldsymbol{x}}_{m,l} + \boldsymbol{e}_l \in \mathbb{C}^{2N}, \quad (1)$$

where

- $\boldsymbol{y}_l^{(\mathrm{P})} \in \mathbb{C}^N$ is the vector of observations collected at the l-th snapshot by the receiving elements with polarization $P \in \{H, V\}$;
- $\bar{\boldsymbol{x}}_{m,l} = \left[\bar{x}_{m,l}^{(\mathrm{H})}, \bar{x}_{m,l}^{(\mathrm{V})}\right]^{\mathrm{T}} \in \mathbb{C}^2$ is the complex polarimetric vector associated with the m-th source amplitudes;
- $$\boldsymbol{S}(\bar{\theta}_m) = \begin{bmatrix} \boldsymbol{s}(\bar{\theta}_m) & \boldsymbol{0} \\ \boldsymbol{0} & \boldsymbol{s}(\bar{\theta}_m) \end{bmatrix} = \boldsymbol{I}_2 \otimes \boldsymbol{s}(\bar{\theta}_m) \in \mathbb{C}^{2N \times 2} \quad (2)$$
  is the polarimetric array matrix[2], with $\boldsymbol{s}(\bar{\theta}_m)$ the unit-norm spatial steering vector of the array at a given polarization for the angular direction $\bar{\theta}_m$;
- $\boldsymbol{e}_l \in \mathbb{C}^{2N}$, $l = 1, \ldots, L$ are independent and identically distributed (i.i.d.) zero-mean circularly symmetric Gaussian random vectors with mean square value η, assumed statistically independent from the sources signals.

Let us now formulate (1) as a linear regression model, whereby the regressors are $\bar{N}$ polarimetric steering matrices $\boldsymbol{S}(\theta_i)$ defined over a grid $\mathbb{T} = \{\theta_i\}_{i=1}^{\bar{N}}$ of the azimuth space. It is worth pointing out that $\mathbb{T}$ is supposed dense enough, i.e., $\bar{N} \gg N$, in order to consider an ideal on-grid scenario, whereby the true DOAs are assumed to belong to $\mathbb{T}$. Hence, the following nonparametric model for the array's output can be considered [21]

$$\boldsymbol{y}_l = \boldsymbol{H}\boldsymbol{x}_l + \boldsymbol{e}_l \in \mathbb{C}^{2N}, \; l = 1, \ldots, L \quad (3)$$

where

- $\boldsymbol{x}_l = \left[\boldsymbol{x}_{1,l}^{\mathrm{T}}, \ldots, \boldsymbol{x}_{\bar{N},l}^{\mathrm{T}},\right]^{\mathrm{T}} \in \mathbb{C}^{2\bar{N}}$, is the sparse vector containing the spatial polarimetric profile for the l-th snapshot, with $\boldsymbol{x}_{i,l} = \left[x_{i,l}^{(\mathrm{H})}, x_{i,l}^{(\mathrm{V})}\right]^{\mathrm{T}} \in \mathbb{C}^2$, $i = 1, \ldots, \bar{N}$;
- $\boldsymbol{H} \in \mathbb{C}^{2N \times 2\bar{N}}$ is the model matrix defined as
$$\boldsymbol{H} = [\boldsymbol{H}_1, \boldsymbol{H}_2, \ldots, \boldsymbol{H}_{\bar{N}}] \quad , \quad (4)$$
with $\boldsymbol{H}_i = \boldsymbol{S}(\theta_i)$ the i-th atom, $i = 1, \ldots, \bar{N}$.

As a matter of fact, the signal model (3) is inherently sparse, as only a few pairs of elements for each vector $\boldsymbol{x}_l$, $l = 1, \ldots, L$, namely only those corresponding to the angles $\bar{\theta}_1, \ldots, \bar{\theta}_K$, are nonzero.

[2]Without loss of generality, in (2) the same steering vectors are considered for both polarizations. However, extensions to the case of different array manifolds for the two polarimetric channels can also be conceived.

That said, by arranging in matrix form the data from all the collected snapshots, the signal model can be conveniently recast as

$$\boldsymbol{Y} = \boldsymbol{H}\boldsymbol{X} + \boldsymbol{E}, \quad (5)$$

where

$$\begin{aligned} \boldsymbol{Y} &= [\boldsymbol{y}_1, \ldots, \boldsymbol{y}_L] \in \mathbb{C}^{2N \times L}, \\ \boldsymbol{X} &= [\boldsymbol{x}_1, \ldots, \boldsymbol{x}_L] \in \mathbb{C}^{2\bar{N} \times L}, \\ \boldsymbol{E} &= [\boldsymbol{e}_1, \ldots, \boldsymbol{e}_L] \in \mathbb{C}^{2N \times L}. \end{aligned} \quad (6)$$

According to (5), the received signal is a linear combination of the columns of $\boldsymbol{H}$, representing the atoms, where the unknown weights $\boldsymbol{X}$ are the sources polarimetric complex amplitudes.

Let us now partition the unknown polarimetric matrix profile $\boldsymbol{X}$ as

$$\boldsymbol{X} = [\boldsymbol{X}_1^{\mathrm{T}}, \ldots, \boldsymbol{X}_{\bar{N}}^{\mathrm{T}}]^{\mathrm{T}} \quad (7)$$

with $\boldsymbol{X}_i = [\boldsymbol{x}_{i,1}, \ldots, \boldsymbol{x}_{i,L}] \in \mathbb{C}^{2\times L}$ the polarimetric signature corresponding to the i-th atom θ_i. It is clear that the signal model (5) presents a direct pathway to retrieve the DOAs as the atoms corresponding to the weights $\boldsymbol{X}_i$ with the strongest norm. Otherwise stated, the space occupancy map recovery process boils down to the determination of the active atoms.

This motivates the design of sparse recovery methods to estimate the unknown profile $\boldsymbol{X}$ so as to get the DOAs, as a by-product. Notably, the estimation process pursued in the following relies on either SLIM or SPICE paradigm. In particular, while in the open literature the atoms in the dictionary are vectors, in this work the signal model (5) demands to consider a generalized atom in the form of a matrix, with the dictionary given by the polarimetric array manifold matrix $\boldsymbol{H}$. However, it is also worth noting that the coherence of such dictionary is the same as the corresponding single-polarization counterpart[3].

III. POLARIMETRIC SPARSE DOA ESTIMATION

In this section, the two approaches proposed to recover the sources' DOAs, i.e., POL-SLIM and POL-SPICE, are developed along with a thoroughly discussion on their convergence features.

A. POL-SLIM

Motivated by the need to exploit multiple snapshots of observations to gather real-time space-frequency electromagnetic awareness, the block version of the SLIM algorithm [19], referred to as Block-SLIM (B-SLIM), is proposed in [20]. Precisely, the approach in [20] resorts to the regularized maximum likelihood estimation paradigm and includes a specific term to promote the inherent sparsity of the overall profile. Here, to account for the polarimetric characteristics of the signals collected by the array (5), the polarimetric

[3]The proof is straightforward being the polarimetric atom structure $\boldsymbol{S}(\theta_i) = \boldsymbol{I}_2 \otimes \boldsymbol{s}(\theta_i)$.

version of the B-SLIM, referred to as POL-SLIM, is developed to obtain the 1-D spatial spectrum profile of the sensed environment. Precisely, the procedure demands the Maximum a Posteriori (MAP) estimate of $\boldsymbol{X}$, η assuming

$$\eta \sim \mathcal{U}(\eta_L, \eta_U) \tag{8}$$

and

$$f_{\boldsymbol{X}}(\boldsymbol{X}) \sim \prod_{i=1}^{\bar{N}} e^{-\frac{2}{q}(\|\boldsymbol{X}_i\|_F^2+\epsilon)^{\frac{q}{2}}}, \tag{9}$$

where $0 < q \leq 1$ rules the sparsity of $\boldsymbol{X}$ (a smaller value of q shrinks toward a higher sparsity of the profile), $\epsilon > 0$ is a smoothing factor [20], and η_L, η_U are respectively a lower and an upper bound to the spectral level of the white interference, with $0 < \eta_L \leq \eta_U$; they could be experimentally evaluated in quasi-ideal (isolated receivers) and stressing (e.g., under peak operating temperature) conditions, respectively [20].

This leads to the formulation of the following minimization problem for block-sparse (with block size $2 \times L$) signal reconstruction[4] [20]

$$\mathcal{P} \begin{cases} \min\limits_{\boldsymbol{X},\eta} & 2NL\log(\eta) + \eta^{-1}\|\boldsymbol{H}\boldsymbol{X} - \boldsymbol{Y}\|_F^2 + f_1(\boldsymbol{X}) \\ \text{s.t.} & \eta_L \leq \eta \leq \eta_U \end{cases}, \tag{10}$$

where

$$f_1(\boldsymbol{X}) = \frac{2}{q}\sum_{i=1}^{\bar{N}}(\|\boldsymbol{X}_i\|_F^2+\epsilon)^{\frac{q}{2}} \tag{11}$$

represents the penalty term promoting sparsity.

The optimization problem (10) may be effectively handled through an iterative procedure based on the block Majorization-Minimization (MM) method [32]–[34], wherein the variables $\boldsymbol{X}$ and η are individually optimized by solving (possibly surrogate) minimization problems. Hence, at a given iteration of the algorithm, the optimization of each variable block is performed keeping the other parameters fixed, with their values set to the estimates computed at the previous iteration. Formally, the n-th iteration of the procedure demands solutions to the following optimization problems:

1) Keeping η fixed, with its value set to $\eta^{(n)}$, the optimization of (10) over the block $\boldsymbol{X}$ yields

$$\min_{\boldsymbol{X}} \frac{\|\boldsymbol{H}\boldsymbol{X} - \boldsymbol{Y}\|_F^2}{\eta^{(n)}} + f_1(\boldsymbol{X}). \tag{12}$$

Exploiting the majorization [20, Appendix A]

$$f_1(\boldsymbol{X}) \leq f_1(\bar{\boldsymbol{X}}) + \|\boldsymbol{D}_{\bar{\boldsymbol{X}}}^P \boldsymbol{X}\|_F^2 - \|\boldsymbol{D}_{\bar{\boldsymbol{X}}}^P \bar{\boldsymbol{X}}\|_F^2, \tag{13}$$

where

- $\bar{\boldsymbol{X}}$ is a problem parameter (set to $\boldsymbol{X}^{(n)}$),
- $\boldsymbol{D}_{\bar{\boldsymbol{X}}}^P = \boldsymbol{D}_{\bar{\boldsymbol{X}}} \otimes \boldsymbol{I}_2$
- $\boldsymbol{D}_{\bar{\boldsymbol{X}}} = \operatorname{diag}\left(\bar{d}_1, \ldots, \bar{d}_{\bar{N}}\right)$
- $\bar{d}_i = \left(\left\|\bar{\boldsymbol{X}}_i\right\|_F^2 + \epsilon\right)^{\frac{q}{4}-\frac{1}{2}}$, $i = 1, \ldots, \bar{N}$,

a solution at the n-th iteration can be obtained by solving the corresponding surrogate minimization problem, namely (see Appendix A for the detailed derivation)

$$\begin{aligned} \boldsymbol{X}^{(n+1)} &= \arg\min_{\boldsymbol{X}} \frac{\|\boldsymbol{H}\boldsymbol{X} - \boldsymbol{Y}\|_F^2}{\eta^{(n)}} + \|\boldsymbol{D}_{\bar{\boldsymbol{X}}}^P \boldsymbol{X}\|_F^2 \\ &= \left(\boldsymbol{H}^\dagger\boldsymbol{H} + \bar{\eta}\boldsymbol{D}_{\bar{\boldsymbol{X}}}^{P\dagger}\boldsymbol{D}_{\bar{\boldsymbol{X}}}^P\right)^{-1}\boldsymbol{H}^\dagger\boldsymbol{Y}. \end{aligned} \tag{14}$$

2) Setting $\boldsymbol{X}$ to $\boldsymbol{X}^{(n+1)}$, and η as the optimization variable, the problem at hand becomes

$$\begin{aligned} \min_{\eta} \quad & 2NL\log(\eta) + \eta^{-1}\left\|\boldsymbol{H}\boldsymbol{X}^{(n+1)} - \boldsymbol{Y}\right\|_F^2 \\ \text{s.t.} \quad & \eta_L \leq \eta \leq \eta_U \end{aligned} \tag{15}$$

whose optimal solution is given by

$$\eta^{(n+1)} = \min\left(\max\left(\eta_L, \check{\eta}\right), \eta_U\right), \tag{16}$$

where

$$\check{\eta} = \frac{1}{2NL}\left\|\boldsymbol{H}\boldsymbol{X}^{(n+1)} - \boldsymbol{Y}\right\|_F^2 \tag{17}$$

Finally, once the estimate $\hat{\boldsymbol{X}}$ of the matrix profile $\boldsymbol{X}$ is obtained, the mean (over the two polarizations) Spatial Power Spectrum (SPS) can be computed as

$$\bar{P}_i = \frac{1}{2L}\|\hat{\boldsymbol{X}}_i\|_F^2, \; i = 1, \ldots, \bar{N} \tag{18}$$

and the DOAs, namely the spatial activation map, can be retrieved from the atoms corresponding to the peaks of the SPS.

As to the selection of the parameter q, several approaches could be considered. One viable method is resorting to a model order selector, such as the Bayesian Information Criterion (BIC) to adaptively choose the appropriate value from a discrete set of points [20], [35]. Alternatively, the value of q can be tuned empirically possibly leveraging some prior knowledge.

That said, an appropriate initialization of the unknowns is also demanded. A wise approach is to employ the matched filter output as the starting point, i.e.,

$$\boldsymbol{X}_i^{(0)} = \boldsymbol{H}_i^\dagger\boldsymbol{Y}, \; i = 1, \ldots, \bar{N} \tag{19}$$

The overall procedure is summarized in **Algorithm 1**, where the exit condition is set as

$$g\left(\boldsymbol{X}^{(n-1)}, \eta^{(n-1)}\right) - g\left(\boldsymbol{X}^{(n)}, \eta^{(n)}\right) \leq \delta \tag{20}$$

with $\delta > 0$ a user-defined parameter and

$$g(\boldsymbol{X}, \eta) = 2NL\log(\eta) + \eta^{-1}\|\boldsymbol{H}\boldsymbol{X} - \boldsymbol{Y}\|_F^2 + f_1(\boldsymbol{X}) \tag{21}$$

the objective function evaluated at $(\boldsymbol{X}, \eta)$.

Remarkably, by invoking [20, Proposition 3.1], two important convergence properties of **Algorithm 1** can be claimed:

1) the sequence of points $(\boldsymbol{X}^{(n)}, \eta^{(n)})$ generated by **Algorithm 1** decreases the objective function in $\mathcal{P}$;

[4]The sensing model and the corresponding sources state inference problem can be extended to accomplish a space-frequency map recovery task, capitalizing also on polarimetric features so as to endow robustness to the environmental state surveillance to the actual unknown sources polarization.

Algorithm 1 POL-SLIM

Input: $\boldsymbol{Y}$, $\boldsymbol{H}$, η_L, η_U, $\epsilon > 0$, $\delta > 0$, and $q \in [0, 1]$.
Initialization. Set $n = 0, \eta^{(0)} = \eta_L$, and
$$\boldsymbol{X}_i^{(0)} = \boldsymbol{H}_i^{\dagger}\boldsymbol{Y},\ i = 1, \ldots, \bar{N}$$
repeat

1) $n = n + 1$
2) $\boldsymbol{D}_{\bar{\boldsymbol{X}}}^{P} = \boldsymbol{D}_{\bar{\boldsymbol{X}}} \otimes \boldsymbol{I}_2$ with
$$\boldsymbol{D}_{\bar{\boldsymbol{X}}} = \operatorname{diag}\left(\|\boldsymbol{X}_1^{(n-1)}\|_F^2 + \epsilon\right)^{\frac{q-2}{4}}, \ldots, \|\boldsymbol{X}_{\bar{N}}^{(n-1)}\|_F^2 + \epsilon\right)^{\frac{q-2}{4}}\Big)$$
3) $\boldsymbol{X}^{(n)} = \left(\boldsymbol{H}^{\dagger}\boldsymbol{H} + \eta^{(n-1)}\boldsymbol{D}_{\bar{\boldsymbol{X}}}^{P\dagger}\boldsymbol{D}_{\bar{\boldsymbol{X}}}^{P}\right)^{-1}\boldsymbol{H}^{\dagger}\boldsymbol{Y}$
4) $\eta^{(n)} = \min\left(\max\left(\eta_L, \check{\eta}\right), \eta_U\right)$ with $\check{\eta} = \frac{1}{2\bar{N}L}\left\|\boldsymbol{H}\boldsymbol{X}^{(n)} - \boldsymbol{Y}\right\|_F^2$

until $g\left(\boldsymbol{X}^{(n-1)}, \eta^{(n-1)}\right) - g\left(\boldsymbol{X}^{(n)}, \eta^{(n)}\right) \leq \delta$
Output. $\hat{\boldsymbol{X}} = \boldsymbol{X}^{(n)}$.

2) any cluster point of the sequence is a Karush-Kuhn-Tucker (KKT) point of $\mathcal{P}$.

B. POL-SPICE

In the previous subsection, the problem of estimating the sparse DOAs has been addressed by directly recovering the signal matrix $\boldsymbol{X}$, an approach extensively explored in the existing literature (e.g., see [36], [37]). However, under the assumption of Gaussian and uncorrelated sources, a statistical learning formulation in terms of covariance matrix estimation could also be pursued [21]. This tailored formulation led (for the single-polarization case) to the development of a practically robust (with respect to (w.r.t.) the sources model assumption) estimator with desirable global convergence properties [21]. For the above reasons, in this subsection the polarimetric version of [21] is derived. To begin with, let us express the data covariance matrix as[5]

$$\boldsymbol{R}(\boldsymbol{P}, \eta) = \mathbb{E}\left[\boldsymbol{Y}\boldsymbol{Y}^{\dagger}\right] = \boldsymbol{H}\boldsymbol{P}\boldsymbol{H}^{\dagger} + \eta\boldsymbol{I}_{2N} = \bar{\boldsymbol{H}}\bar{\boldsymbol{P}}\bar{\boldsymbol{H}}^{\dagger}, \quad (22)$$

where

$$\bar{\boldsymbol{H}} = [\boldsymbol{H}, \boldsymbol{I}_{2N}] \in \mathbb{C}^{2N \times (2\bar{N}+2N)}, \quad (23)$$

and

$$\bar{\boldsymbol{P}} = \operatorname{diag}(\boldsymbol{P}, \eta\boldsymbol{I}_{2N}) \in \mathbb{R}^{(2\bar{N}+2N)\times(2\bar{N}+2N)}, \quad (24)$$

with $\boldsymbol{P} = \operatorname{diag}([\boldsymbol{P}_1, \ldots, \boldsymbol{P}_{\bar{N}}]) = \mathbb{E}[\boldsymbol{X}\boldsymbol{X}^{\dagger}] \in \mathbb{R}^{2\bar{N}\times 2\bar{N}}$ and $\boldsymbol{P}_i \in \mathbb{R}^{2\times 2}$ the polarimetric covariance matrix of the i-th source related to the i-th atom.

Using the SPICE criterion, the estimation problem at hand could be addressed by minimizing the following covariance fitting performance metric [21]

$$\begin{cases} \left\|\boldsymbol{R}^{-\frac{1}{2}}\left(\boldsymbol{R}_{SCM} - \boldsymbol{R}\right)\right\|_F^2 & L < 2N \\ \left\|\boldsymbol{R}^{-\frac{1}{2}}\left(\boldsymbol{R}_{SCM} - \boldsymbol{R}\right)\boldsymbol{R}_{SCM}^{-\frac{1}{2}}\right\|_F^2 & L \geq 2N \end{cases}, \quad (25)$$

where $\boldsymbol{R}_{SCM} = \frac{1}{L}\boldsymbol{Y}\boldsymbol{Y}^{\dagger}$ is the sample covariance matrix. However, if (25) is adopted as objective function, then two remarks are necessary. First, it involves distinction between the cases $L < 2N$ and $L \geq 2N$ like in [18] for the single-polarization scenario. Second, the resulting optimization problem can possibly be not well-posed for the $L = 1$ (see Appendix B), which is a crucial scenario for radar applications. Therefore, in order to work with only one objective function which would guarantee that the covariance matrix estimation problem is well-posed, regardless of the number of snapshots (with $L \geq 1$), along with a unifying treatment, the Fast ML (FML) estimate of the covariance matrix is employed in lieu of $\boldsymbol{R}_{SCM}$. Precisely, the FML procedure [38], [39] provides the ML Estimation (MLE) when $\boldsymbol{R}$ belongs to the uncertainty set of positive definite matrices whose eigenvalues are greater than or equal to a specific value, that is, under the assumption that a lower bound η_L on the thermal noise power level is a-priori available. Therefore, denoting by $\boldsymbol{U}\boldsymbol{\Lambda}\boldsymbol{U}^{\dagger}$ the Eigenvalue Decomposition (EVD) of $\boldsymbol{R}_{SCM}$ and by $\tilde{\lambda}_v,\ v = 1, \ldots, N$ its eigenvalues, the FML estimate is given by

$$\tilde{\boldsymbol{R}} = \boldsymbol{U}\boldsymbol{\Lambda}_{FML}\boldsymbol{U}^{\dagger}, \quad (26)$$

where

$$\boldsymbol{\Lambda}_{FML} = \operatorname{diag}(\lambda_{1,FML}, \ldots, \lambda_{N,FML}) \quad (27)$$

with $\lambda_{v,FML} = \max(\tilde{\lambda}_v,\ \eta_L),\ v = 1, \ldots, N$.

This technique ensures that all the eigenvalues of $\tilde{\boldsymbol{R}}$ are greater than or equal to the lower bound on the power noise level. Notably, this estimation process is equivalent to perform the projection (in terms of Frobenius norm) of $\boldsymbol{R}_{SCM}$ onto the set of the positive definite matrices greater than or equal to $\eta_L\boldsymbol{I}$ [40].

Leveraging (26), the considered objective function is given by

$$\left\|\boldsymbol{R}^{-\frac{1}{2}}\left(\tilde{\boldsymbol{R}} - \boldsymbol{R}\right)\tilde{\boldsymbol{R}}^{-\frac{1}{2}}\right\|_F^2 \quad (28)$$

which, after algebraic manipulation, can be rewritten as

$$\mathcal{P}_1 \begin{cases} \min\limits_{\boldsymbol{P}\succ\boldsymbol{0}, \eta_L \leq \eta \leq \eta_U} & \operatorname{tr}(\boldsymbol{R}^{-1}\tilde{\boldsymbol{R}}) + \sum\limits_{i=1}^{\bar{N}} \operatorname{tr}(\boldsymbol{H}_i^{\dagger}\tilde{\boldsymbol{R}}^{-1}\boldsymbol{H}_i\boldsymbol{P}_i) \\ & + \eta\operatorname{tr}(\tilde{\boldsymbol{R}}^{-1}) \end{cases}. \quad (29)$$

Remarkably, $\mathcal{P}_1$ is jointly convex w.r.t. $\boldsymbol{P}_i$ and η; thus, it can be solved via any Semi-Definite Program (SDP) solver, with the drawback (due to the high dimensionality of the problem) of a high computational complexity [41]. Therefore, an efficient and iterative optimization procedure

[5]For ease of notation, the matrix $\boldsymbol{R}(\boldsymbol{P}, \eta)$ is referred to in the following as $\boldsymbol{R}$.

is devised as follows. First of all, let us equivalently[6] reformulate (29) as [21]

$$\mathcal{P}_2 \left\{ \begin{array}{cc} \min\limits_{\boldsymbol{C},\boldsymbol{P}\succ\boldsymbol{0},\eta_L\leq\eta\leq\eta_U} & f(\boldsymbol{C},\boldsymbol{P},\eta) \\ \text{s.t.} & \bar{\boldsymbol{H}}\boldsymbol{C}=\tilde{\boldsymbol{R}}^{\frac{1}{2}} \end{array} \right. \tag{30}$$

with $\boldsymbol{C}\in\mathbb{C}^{(2\bar{N}+2N)\times 2N}$ a slack variable and

$$\begin{aligned} f(\boldsymbol{C},\boldsymbol{P},\eta) =& \operatorname{tr}(\boldsymbol{C}^\dagger\bar{\boldsymbol{P}}^{-1}\boldsymbol{C})+\sum_{i=1}^{\bar{N}}\operatorname{tr}(\boldsymbol{H}_i^\dagger\tilde{\boldsymbol{R}}^{-1}\boldsymbol{H}_i\boldsymbol{P}_i) \\ &+\eta\operatorname{tr}(\tilde{\boldsymbol{R}}^{-1}) \end{aligned} \tag{31}$$

the objective function to optimize. Hence, resorting to the Coordinate Descent (CD) framework, at the n-th iteration, each block variable, i.e., $\boldsymbol{C}$, $\boldsymbol{P}$, and η, is optimized at a time while keeping the others fixed. Notably, each sub-problem can be solved in closed-form, yielding the following CD updating rules (see Appendix C)

$$\boldsymbol{C}^{(n)}=\bar{\boldsymbol{P}}^{(n)}\bar{\boldsymbol{H}}^\dagger(\boldsymbol{R}^{(n)})^{-1}\tilde{\boldsymbol{R}}^{\frac{1}{2}}, \tag{32}$$

$$\boldsymbol{P}^{(n)}=\operatorname{diag}([\boldsymbol{P}_1^{(n)},\ldots,\boldsymbol{P}_{\bar{N}}^{(n)}]), \tag{33}$$

and

$$\eta^{(n)}=\min\left(\max\left(\eta_L,\check{\eta}\right),\eta_U\right), \tag{34}$$

where

$$\check{\eta}=\sqrt{\frac{\sum\limits_{i=\bar{N}+1}^{\bar{N}+N}\left\|\boldsymbol{C}_i^{(n)}\right\|_F^2}{\operatorname{tr}(\tilde{\boldsymbol{R}}^{-1})}} \tag{35}$$

and, for $i=1,\ldots,\bar{N}$,

$$\boldsymbol{P}_i^{(n)}=\boldsymbol{Z}_i\left[\boldsymbol{Z}_i^{-1}\left(\boldsymbol{H}_i^\dagger\tilde{\boldsymbol{R}}^{-1}\boldsymbol{H}_i\right)^{-1}\boldsymbol{Z}_i^{-1}\right]^{\frac{1}{2}}\boldsymbol{Z}_i, \tag{36}$$

with

$$\boldsymbol{Z}_i=\left(\boldsymbol{C}_i^{(n)}\boldsymbol{C}_i^{(n)\dagger}\right)^{\frac{1}{2}}. \tag{37}$$

and $\boldsymbol{C}_i\in\mathbb{C}^{2\times 2N}$ obtained by extracting the $(2i-1)$-th and $(2i)$-th rows of $\boldsymbol{C}$. The devised POL-SPICE procedure is reported in **Algorithm 2** whereby the polarimetric covariance matrix is initialized as $\boldsymbol{P}_i^{(0)}=\tilde{\boldsymbol{X}}_i\tilde{\boldsymbol{X}}_i^\dagger$ with $\tilde{\boldsymbol{X}}_i=\boldsymbol{H}_i^\dagger\boldsymbol{Y}/\sqrt{L}$, $i=1,\ldots,\bar{N}$, while the exit condition is set as

$$\frac{\|\boldsymbol{P}^{(n)}-\boldsymbol{P}^{(n-1)}\|_F}{\|\boldsymbol{P}^{(n-1)}\|_F}\leq\delta. \tag{38}$$

As a final remark, the convergence properties of **Algorithm 2** is analyzed. To begin with, observe that the following conditions are satisfied

- C1) $f(\boldsymbol{C},\boldsymbol{P},\eta)$ is continuously differentiable over the feasible set;
- C2) each subproblem has an unique solution (which is computed in closed-form);
- C3) each block variable is optimized over a compact set (see Appendix D);

[6]Denoting by $\hat{\boldsymbol{C}}$, $\hat{\boldsymbol{P}}$, and $\hat{\eta}$ the optimal solution to $\mathcal{P}_2$, it is straightforward to prove that $(\hat{\boldsymbol{P}},\hat{\eta})$ is the optimal solution to $\mathcal{P}_1$ as well [21].

Algorithm 2 POL-SPICE

Input: $\boldsymbol{Y}$, $\boldsymbol{H}$, $\tilde{\boldsymbol{R}}^{-1}$, $\tilde{\boldsymbol{R}}^{\frac{1}{2}}$, η_L, η_U, and $\delta>0$.
Initialization. Set $n=0,\eta^{(0)}=\eta_L$, $\bar{\boldsymbol{H}}=[\boldsymbol{H},\boldsymbol{I}_{2N}]$ and $\boldsymbol{P}_i^{(0)}=\tilde{\boldsymbol{X}}_i\tilde{\boldsymbol{X}}_i^\dagger$ with $\tilde{\boldsymbol{X}}_i=\boldsymbol{H}_i^\dagger\boldsymbol{Y}/\sqrt{L}$, $i=1,\ldots,\bar{N}$
repeat

1) $n=n+1$
2) $\bar{\boldsymbol{P}}^{(n)}=\operatorname{diag}(\boldsymbol{P}^{(n-1)},\eta^{(n-1)}\boldsymbol{I}_{2N})$
3) $\boldsymbol{R}^{(n)}=\bar{\boldsymbol{H}}\bar{\boldsymbol{P}}^{(n)}\bar{\boldsymbol{H}}^\dagger$
4) $\boldsymbol{C}^{(n)}=\bar{\boldsymbol{P}}^{(n)}\bar{\boldsymbol{H}}^\dagger(\boldsymbol{R}^{(n)})^{-1}\tilde{\boldsymbol{R}}^{\frac{1}{2}}$
5) $\eta^{(n)}=\min\left(\max\left(\eta_L,\check{\eta}\right),\eta_U\right)$ with $\check{\eta}=\sqrt{\frac{\sum_{i=\bar{N}+1}^{\bar{N}+N}\|\boldsymbol{C}_i^{(n)}\|_F^2}{\operatorname{tr}(\tilde{\boldsymbol{R}}^{-1})}}$
6) $\boldsymbol{P}^{(n)}=\operatorname{diag}([\boldsymbol{P}_1^{(n)},\ldots,\boldsymbol{P}_{\bar{N}}^{(n)}])$ where, for $i=1,\ldots,\bar{N}$

$$\boldsymbol{P}_i^{(n)}=\boldsymbol{Z}_i\left[\boldsymbol{Z}_i^{-1}\left(\boldsymbol{H}_i^\dagger\tilde{\boldsymbol{R}}^{-1}\boldsymbol{H}_i\right)^{-1}\boldsymbol{Z}_i^{-1}\right]^{\frac{1}{2}}\boldsymbol{Z}_i,$$

with

$$\boldsymbol{Z}_i=\left(\boldsymbol{C}_i^{(n)}\boldsymbol{C}_i^{(n)\dagger}\right)^{\frac{1}{2}}.$$

until $\|\boldsymbol{P}^{(n)}-\boldsymbol{P}^{(n-1)}\|_F/\|\boldsymbol{P}^{(n-1)}\|_F\leq\delta$
Output. $\bar{P}_i=\|\boldsymbol{P}_i^{(n)}\|_F$, $i=1,\ldots,\bar{N}$.

- C4) $f(\boldsymbol{C},\boldsymbol{P},\eta)$ is jointly convex over its block components.

As a consequence, due to [33, Theorem 2], any limit point of the iterates generated by **Algorithm 2** is a stationary point of $\mathcal{P}_2$ and, due to C4), it is also a global minimum of $f(\boldsymbol{C},\boldsymbol{P},\eta)$ [42].

IV. PERFORMANCE ANALYSIS

In order to evaluate the performance of the proposed estimation procedures, two scenarios of practical relevance are considered in the following. The former refers to a passive sensing configuration, whereas the latter investigates the performance of an active polarimetric radar operating in the presence of multipath. In the simulations, unless otherwise specified, the dictionary is built as a discretization of the azimuth domain $[-\pi/2,\pi/2]$ with $\bar{N}=1000$ equally spaced points.

A. PASSIVE SENSING SCENARIO

Let us consider a passive sensor equipped with $N=35$ crossed dipoles, arranged in a standard Uniform Linear Array (ULA) configuration, receiving data in both horizontal and vertical polarizations. It is assumed that the system collects $L=200$ snapshots in the presence of $K=3$ uncorrelated Gaussian sources impinging on the sensor from azimuth directions $\bar{\boldsymbol{\theta}}=[-18.11,-14.50,17.93]^\circ$, which correspond to the positions $[400,420,600]$ of the atoms within the dictionary. Precisely, at the l-th snapshot, the received signal

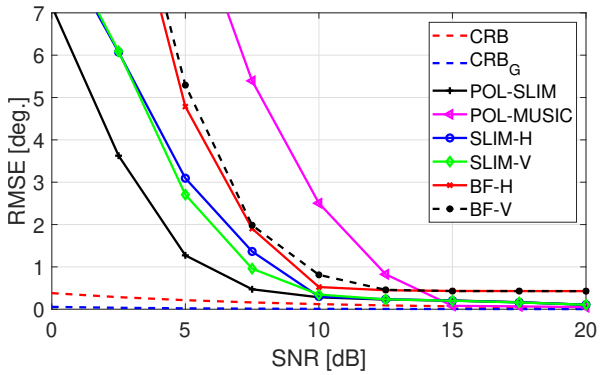

(a)

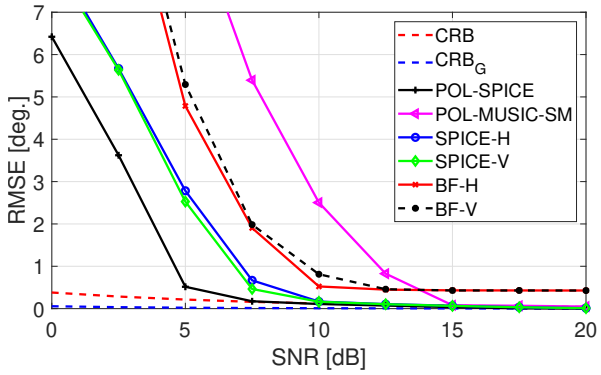

(b)

FIGURE 1: RMSE vs SNR for $L = 200$, $\rho = 0.5$, and $\sigma_c = 0.9$. (a) SLIM-based procedures vs counterparts. (b) SPICE-based procedures vs counterparts.

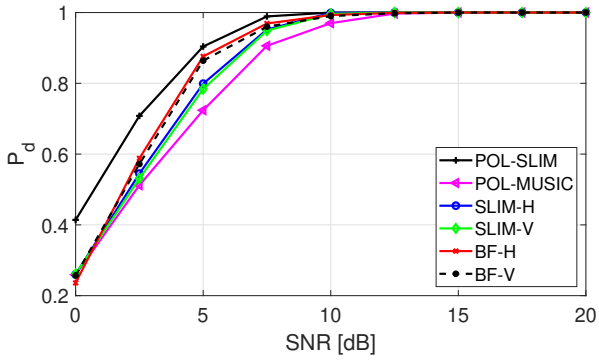

(a)

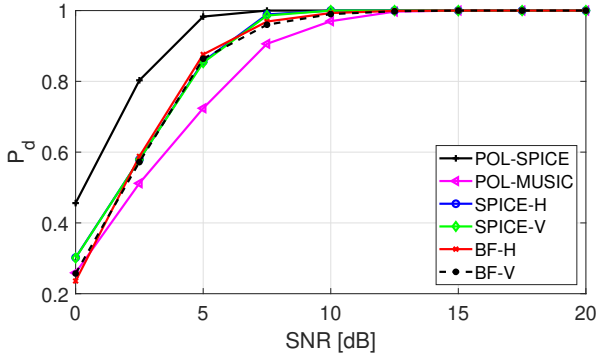

(b)

FIGURE 2: $\mathrm{P_d}$ vs SNR for $L = 200$, $\rho = 0.5$, and $\sigma_c = 0.9$. (a) SLIM-based procedures vs counterparts. (b) SPICE-based procedures vs counterparts.

is given by (1), with the emitters (independent of each other) complex amplitudes on the two polarizations modeled as

$$\bar{\boldsymbol{x}}_{m,l} \sim CN(0, |\alpha|^2 \boldsymbol{M}_m),\ l = 1, \ldots, L,\ m = 1, \ldots, K \tag{39}$$

where

$$\boldsymbol{M}_m = P_m \boldsymbol{\Sigma}_j \tag{40}$$

with $P_1 = 1$, $P_2 = 9$, $P_3 = 4$, and

$$\boldsymbol{\Sigma}_j = \begin{bmatrix} 1-\rho & \sigma_c\sqrt{\rho(1-\rho)} \\ \sigma_c\sqrt{\rho(1-\rho)} & \rho \end{bmatrix}, \tag{41}$$

while ρ represents the polarimetric power imbalance coefficient, and σ_c is the polarimetric correlation coefficient.

The SNR is defined as

$$\mathrm{SNR} = \frac{|\alpha|^2}{\eta} \frac{1}{K} \mathrm{tr}(\boldsymbol{P}), \tag{42}$$

where η is assumed, without loss of generality, equal to 0 dB and

$$\boldsymbol{P} = \mathrm{diag}([P_1, P_2, P_3]^{\mathrm{T}}). \tag{43}$$

The CRB for either unknown nonrandom sources or for unknown Gaussian sources (referred to as $\mathrm{CRB_G}$), whose derivations are provided in Appendix E, is reported as benchmark while the following counterparts are included for comparison purposes:

- the CBF using a single-polarization subarray (either working in H or V polarization) [3];
- the block-sparse single-polarization SLIM and SPICE algorithms [18], [20], [21];
- an extension of the MUSIC algorithm (referred to in the following as POL-MUSIC) for crossed-dipoles arrays (see Appendix F).

The angular estimation performance of the considered methods is assessed using two figures of merit, i.e.,

- the Root Mean Square Error (RMSE) computed as

$$\widehat{\mathrm{RMSE}} = \sqrt{\frac{1}{\mathrm{MC}} \sum_{l=1}^{\mathrm{MC}} \frac{1}{K} \sum_{m=1}^{K} |\hat{\theta}_{m,l} - \bar{\theta}_m|^2}, \tag{44}$$

  where $\hat{\theta}_{m,l}$ is the m-th source DOA estimate at the l-th trial with $\mathrm{MC} = 1000$ the number of Monte Carlo trials;
- the probability of detecting the sources within 1.8 degrees from the true DOAs (denoted as $\mathrm{P_d}$).

Furthermore, the POL-SLIM has been implemented as a two-step procedure. First, a spatial spectrum is inferred

This article has been accepted for publication in IEEE Open Journal of Signal Processing. This is the author's version which has not been fully edited and content may change prior to final publication. Citation information: DOI 10.1109/OJSP.2024.3411468

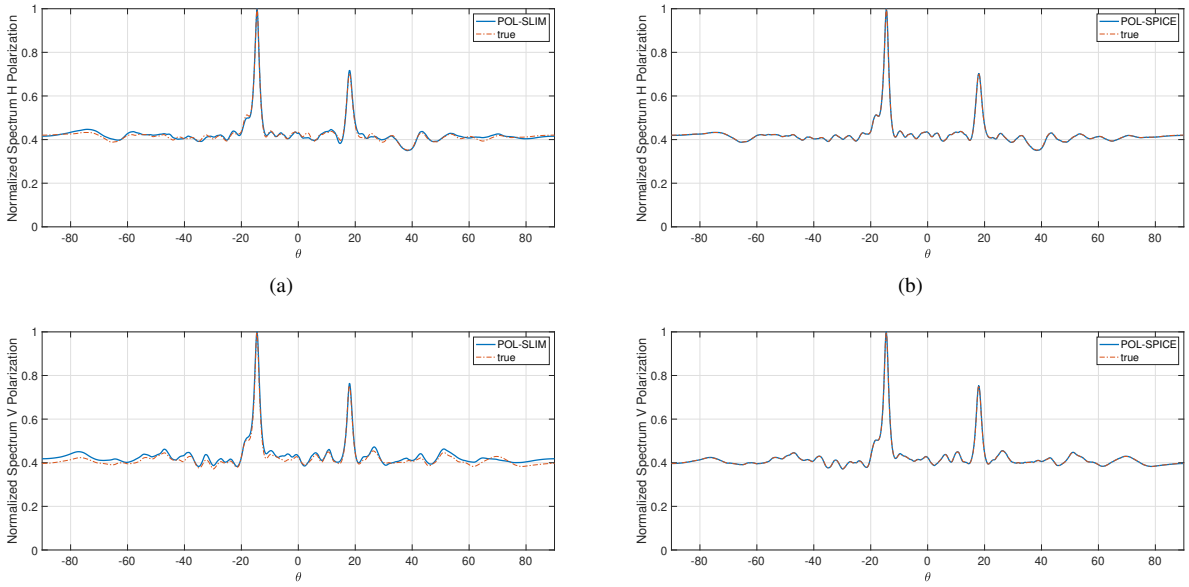

FIGURE 3: Capon spectrum (45), normalized to the maximum, computed for $\rho = 0.5$, $\sigma_c = 0.9$, and SNR = 7 dB, using the single-polarization covariance matrix estimated by either POL-SLIM or POL-SPICE method. Figs. (a) and (b) report the spectra in H polarization, whereas the curves in Figs. (c) and (d) refer to V polarization.

adopting $q = 1$; then, the estimated sparse profile is used to initialize a second POL-SLIM process with $q = 0.5$, aimed at further promoting the sparsity of the results and refining the DOA inference process.

The simulation results, reported in Figs. 1 and 2 for $\rho = 0.5$ and $\sigma_c = 0.9$, show that POL-SLIM and POL-SPICE outperform the corresponding single-polarization algorithms, the CBF as well as POL-MUSIC, in terms of both RMSE and $\mathrm{P_d}$. Precisely, for SNR $= 5$ dB, the devised techniques are capable of providing RMSE values in the order of 1 degree, with an appreciable improvement (of approximately 2 degrees) compared to their single-polarization counterparts. Moreover, they approach the CRB at lower SNR values than all the other considered estimators. Under low/medium SNR regime (and in particular for SNR values smaller than 15 dB), POL-MUSIC achieves lower estimation performance than the counterparts (even those working in single polarization). However, in the high SNR regime, it is able to attain the CRB as well as $\mathrm{P_d} = 1$.

Additionally, Fig. 2 highlights that POL-SLIM and POL-SPICE are capable of providing higher $\mathrm{P_d}$ than the other methods. In particular, at $\mathrm{P_d} = 0.9$, there is a performance gain of approximately 1 dB for POL-SLIM and 2 dB for POL-SPICE when compared to the single-polarization counterparts.

Notably, for the employed simulation parameters, a direct comparison between the two polarimetric methods reveals that, for a given SNR, POL-SPICE consistently provides more accurate DOA estimates as well as higher $\mathrm{P_d}$ values than POL-SLIM. The observed superiority is likely a consequence of the fact that POL-SPICE operates under a model matching condition of the procedure, as the analyzed case is characterized by the presence of uncorrelated Gaussian sources.

Aimed at providing a further insight into the effectiveness of the developed approaches, Figs. 3 and 4 report, for a specific trial instance and for SNR=7 dB and SNR=15 dB, respectively, the estimated single-polarization spectra $\check{\boldsymbol{x}}^{(P)}$, normalized to its maximum. Precisely, the i-th element of $\check{\boldsymbol{x}}^{(P)}$, corresponding to the spectrum at the angle θ_i, is estimated by the Capon formula

$$\check{\boldsymbol{x}}^{(P)}(i) = \frac{1}{L}\sum_{l=1}^{L}\left|\frac{\boldsymbol{s}(\theta_i)^\dagger \check{\boldsymbol{R}}_P^{-1}\boldsymbol{y}_l^{(\mathrm{P})}}{\boldsymbol{s}(\theta_i)^\dagger \check{\boldsymbol{R}}_P^{-1}\boldsymbol{s}(\theta_i)}\right|, \quad \begin{array}{c} i = 1,\ldots,\bar{N} \\ P \in \{H,V\} \end{array} \tag{45}$$

where, $\check{\boldsymbol{R}}_P = \bar{\boldsymbol{A}}\bar{\boldsymbol{P}}^{(P)}\bar{\boldsymbol{A}}^\dagger$ is the estimated covariance matrix at the given polarization P, with $\bar{\boldsymbol{A}} = [\boldsymbol{s}(\theta_1),\ldots,\boldsymbol{s}(\theta_{\bar{N}}), \boldsymbol{I}_N]$ the extended single-polarization dictionary and $\bar{\boldsymbol{P}}^{(P)}$ the corresponding power estimated by either POL-SLIM or POL-SPICE. In the figures, the estimated profile is compared with the true one, i.e., the Capon spectrum (45) computed using the true single-polarization covariance matrices. The results highlight that the estimated profiles achieve a good match with the theoretical counterparts at both SNR equal to 7 dB and 15 dB.

Figs. 5 and 6 report the RMSE and Pd versus SNR curves, respectively, for the case of $\rho = 0.6$ and $\sigma_c = 0.4$. Unlike the previous case study, characterized by equal signal power distribution among the two polarimetric channels, this

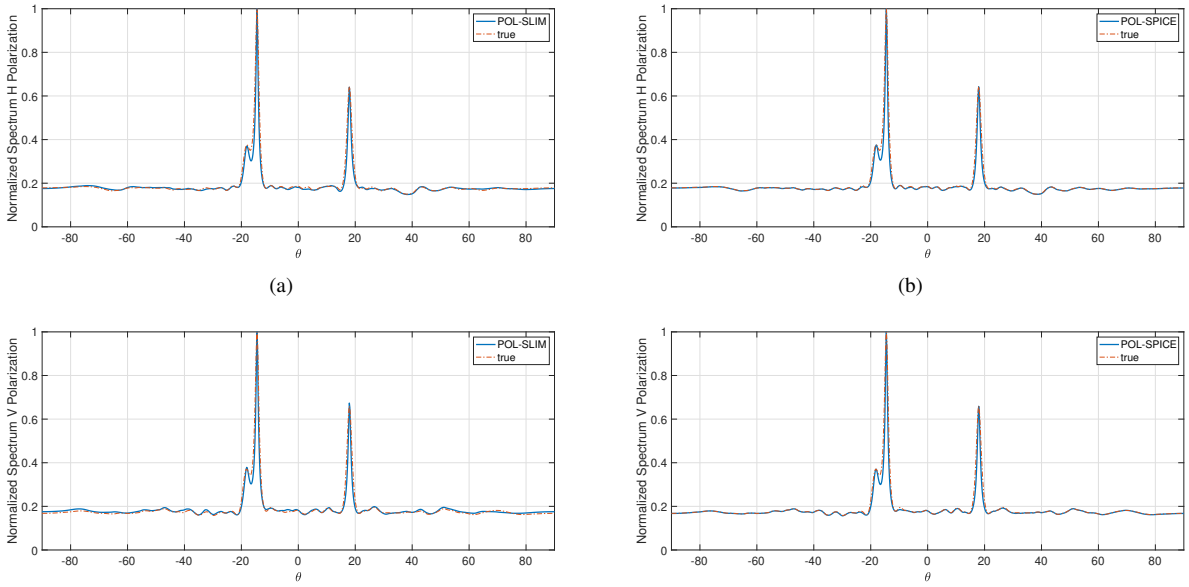

FIGURE 4: Capon spectrum (45), normalized to the maximum, computed for $\rho = 0.5$, $\sigma_c = 0.9$, and SNR = 15 dB, using the single-polarization covariance matrix estimated by either POL-SLIM or POL-SPICE method. Figs. (a) and (b) report the spectra in H polarization, whereas the curves in Figs. (c) and (d) refer to V polarization.

scenario reveals a noticeable performance gap between the performance of single polarization methods operating on H and V polarization data. In fact, at SNR = 5 dB, it is possible to observe a RMSE difference of about 1.5 degrees between SLIM-H and SLIM-V and similarly of 2 degrees between SPICE-H and SPICE-V. On the other hand, the proposed polarimetric estimation strategies yield the best performance among all the considered counterparts, thus demonstrating their effectiveness in exploiting the polarimetric characteristics of the received signals. As a consequence, such methods endow robustness to the environmental awareness process against possible power mismatches and/or correlation among the polarimetric channels. It is worth noting that, in a typical passive sensing scenario, the received power distribution among the two polarization channels is generally unknown; therefore, single-polarization methods using data from the weak polarimetric channel may experience a considerable performance degradation. In contrast, POL-SLIM and POL-SPICE consistently maintain satisfactory performance without requiring prior information about signal power distribution on the two polarimetric channels.

Finally, Figs. 7 and 8 illustrate the results, in terms of RMSE vs ρ and $\mathrm{P_d}$ vs ρ, respectively, achieved by the SLIM-based and SPICE-based procedures for SNR = 10 dB, $L = 200$, and $\sigma_c = 0.9$. Inspection of the curves highlights that when $\rho = 0$, i.e., the returns on the H polarization are dominant, the methods that exploit the data collected on the H channel are capable of providing $\mathrm{P_d}$ close to 1 and estimation accuracy in the order of 0.5°. On the other hand, the single polarization methods employing data obtained on the V channel fail to accomplish the detection task (with $\mathrm{P_d}$ approximately 0). However, the performance of such data processors employing H (V) polarization data is degraded (improved) as ρ increases. Moreover, regardless of the employed polarimetric channel, all the single-pol methods achieve similar results (in terms of comparing each H-pol method with the corresponding V-pol counterpart) in the case of $\rho = 0.5$. Notably, the proposed POL-SLIM and POL-SPICE consistently exhibit the best performance among all the reported methods, regardless of the value of ρ. This behavior further corroborates the advantage of the devised techniques toward an effective exploitation of the polarimetric domain and thus providing robust performance with respect to any unknown polarimetric power imbalance.

B. RADAR SCENARIO

In this subsection, a typical radar application is considered, wherein a radar aims at estimating the elevation of a prospective target in the presence of a vertical multipath. In this context, considering the radar transmitting a single pulse (i.e., $L = 1$) on polarization H and assuming a rather smooth reflection surface [43], at the listening stage it receives two useful signal contributions on each polarization channel, namely the target echo from the direct path as well as the multipath [1], as shown in Fig. 9 (with the array elements arranged along the y-axis), where

- $\bar{\theta}_d$ is target elevation;
- $\bar{\theta}_s$ is reflection angle;

This article has been accepted for publication in IEEE Open Journal of Signal Processing. This is the author's version which has not been fully edited and content may change prior to final publication. Citation information: DOI 10.1109/OJSP.2024.3411468

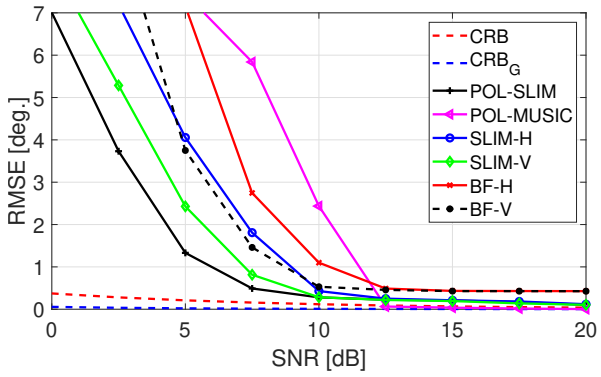

(a)

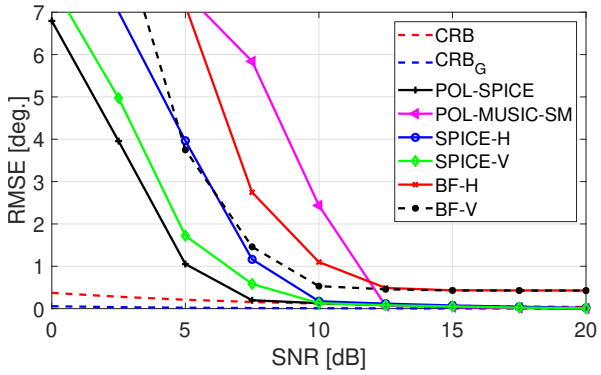

(b)

FIGURE 5: RMSE vs SNR for $L = 200$, $\rho = 0.6$, and $\sigma_c = 0.4$. (a) SLIM-based procedures vs counterparts. (b) SPICE-based procedures vs counterparts.

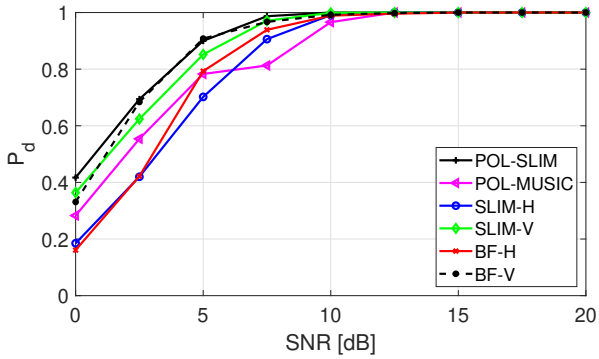

(a)

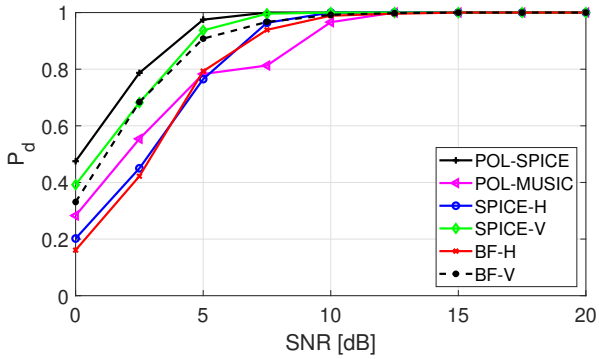

(b)

FIGURE 6: $\mathrm{P_d}$ vs SNR for $L = 200$, $\rho = 0.6$, and $\sigma_c = 0.4$. (a) SLIM-based procedures vs counterparts. (b) SPICE-based procedures vs counterparts.

- $R_d = [R^2 + (h_t - h_r)^2]^{\frac{1}{2}}$ and $R_s = [R^2 + (h_t + h_r)^2]^{\frac{1}{2}}$ are the direct (slant range) and reflected path distance, respectively;
- h_t and h_r are the receiver and the target height, respectively,

with R the ground distance between the target and the receiver. In this regard, the following relationship holds true [43]

$$\bar{\theta}_s = -\arctan\left(\tan(\bar{\theta}_d) + \frac{2h_r}{R}\right). \tag{46}$$

Within the aforementioned geometry, the received signal can be modeled as

$$\begin{aligned}\boldsymbol{y} &= \left[\boldsymbol{y}^{(\mathrm{H})\mathrm{T}}, \boldsymbol{y}^{(\mathrm{V})\mathrm{T}}\right]^{\mathrm{T}} \\ &= \left[\boldsymbol{S}(\bar{\theta}_d), \boldsymbol{S}(\bar{\theta}_s)\right] \left[x_H, x_V, \rho_H x_H e^{-j\phi}, \rho_V x_V e^{-j\phi}\right]^{\mathrm{T}} \\ &\quad + \boldsymbol{e} \in \mathbb{C}^{2N},\end{aligned} \tag{47}$$

where

- $\boldsymbol{x} = [x_H, x_V]^T \in \mathbb{C}^2$ is the polarimetric complex target echo amplitude, modeled as a zero-mean complex circular Gaussian random vector with covariance matrix $\gamma \boldsymbol{M}_T$, whereas $\boldsymbol{M}_T$ is given by [44]

$$\boldsymbol{M}_T = \sigma_P \begin{bmatrix} 1 & \rho_P \sqrt{\gamma_P} \\ \rho_P^\star \sqrt{\gamma_P} & \gamma_P \end{bmatrix} \tag{48}$$

  and the values of σ_P, ρ_P, and γ_P, namely the target polarimetric parameters, are reported in Table 1;
- ρ_H and ρ_V are the ground reflection coefficients in polarization H and V, respectively;
- $\phi = 2\pi\Delta R/\lambda$ is the phase shift induced by the additional path (i.e., ΔR) traveled by the reflected signal w.r.t. the direct one;
- $\boldsymbol{e}$ is a zero-mean circularly symmetric Gaussian random vector with mean square value η, independent from $\boldsymbol{x}$,

whereas the SNR is modeled as $\mathrm{SNR} = \gamma/\eta$.

In the considered case study characterized by an approximately flat surface, the ground reflection coefficients can be modeled according to [43] as

$$\begin{aligned}\rho_H &= \frac{\sin\left(-\bar{\theta}_s\right) - \sqrt{\varepsilon - \left(\cos\left(\bar{\theta}_s\right)\right)^2}}{\sin\left(-\bar{\theta}_s\right) + \sqrt{\varepsilon - \left(\cos\left(\bar{\theta}_s\right)\right)^2}} \\ \rho_V &= \frac{\varepsilon\sin\left(-\bar{\theta}_s\right) - \sqrt{\varepsilon - \left(\cos\left(\bar{\theta}_s\right)\right)^2}}{\varepsilon\sin\left(-\bar{\theta}_s\right) + \sqrt{\varepsilon - \left(\cos\left(\bar{\theta}_s\right)\right)^2}}\end{aligned} \tag{49}$$

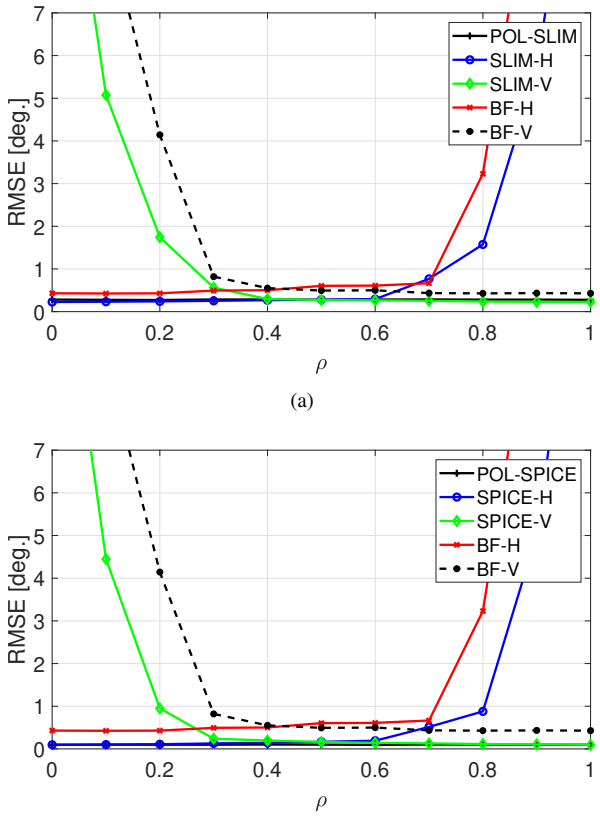

FIGURE 7: RMSE vs ρ for SNR = 10 dB, $L = 200$, and $\sigma_c = 0.9$. (a) SLIM-based procedures vs counterparts. (b) SPICE-based procedures vs counterparts.

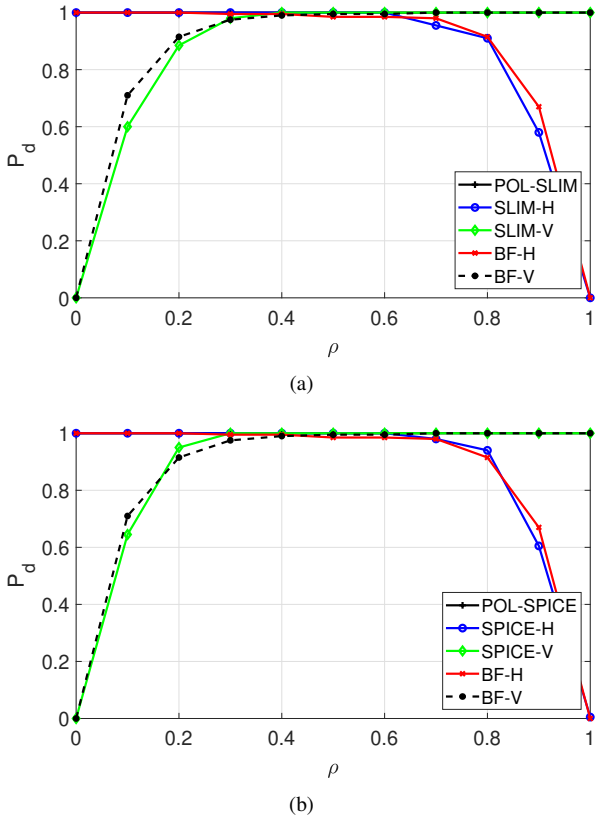

FIGURE 8: P_d vs ρ for SNR = 10 dB, $L = 200$, and $\sigma_c = 0.9$. (a) SLIM-based procedures vs counterparts. (b) SPICE-based procedures vs counterparts.

where

$$\varepsilon = \varepsilon_r - \mathrm{j}60\lambda\sigma_e \tag{50}$$

is the complex permittivity, with ε_r and σ_e the relative permittivity and the surface conductivity, respectively.

The simulation parameters are provided in Table 1 whereby, for the ground model, it is assumed a typical ordinary soil surface [43]. In particular, $\bar{\theta}_d = 3°$ and $\bar{\theta}_s = -3.76°$, with an angular separation between the two paths of $6.76°$.

In this case study, the RMSE of the target DOA $\bar{\theta}_d$ is considered as a figure of merit, i.e.,

$$\widehat{\mathrm{RMSE}} = \sqrt{\frac{1}{\mathrm{MC}} \sum_{l=1}^{\mathrm{MC}} |\hat{\theta}_l - \bar{\theta}_d|^2}, \tag{51}$$

where $\hat{\theta}_l$ is the estimated target DOA (obtained as the peak of the spatial spectra obtained by the considered SLIM-based and SPICE-based procedures) at the l-th trial. Moreover, it is worth noting that, since the modulus of the reflection coefficients are $|\rho_H| = 0.97$ and $|\rho_V| = 0.58$, in V polarization the direct return is significantly stronger than the reflected return, whereas in H polarization the two contributions have similar amplitudes.

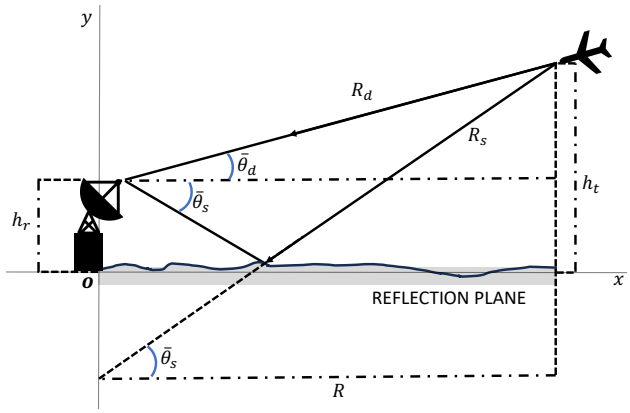

FIGURE 9: Setup geometry for the simulation scenario considered in subsection B.

The estimation performance for the aforementioned radar scenario is reported in Fig. 10 in terms of RMSE versus SNR. Inspection of the curves reveals that, under a low/medium SNR regime (SNR < 10 dB), SLIM and SPICE methods perform better in H polarization than the V one, as the returns in the former channel are stronger than in the latter (recall that $\gamma_P = 0.1$). Conversely, at high SNR, it is more advantageous to employ the data collected in V

TABLE 1: Simulation parameters for subsection B.

Parameter	Value	Parameter	Value
f	145 MHz	R	30 km
h_r	200 m	h_t	1 km
$\bar{\theta}_d$	3°	$\bar{\theta}_s$	-3.76°
ε_r	15	σ_e	0.005
σ_P	58.5	γ_P	0.1
ρ_P	0.885	η	0 dB

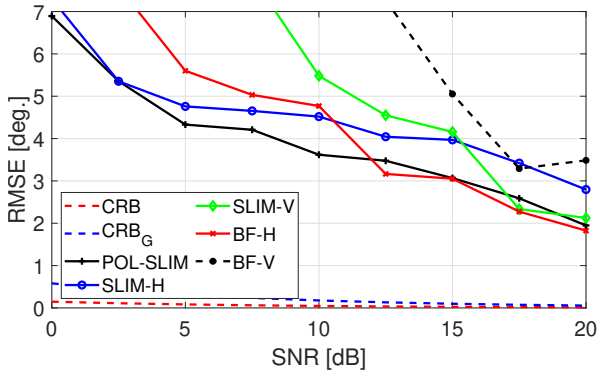

(a)

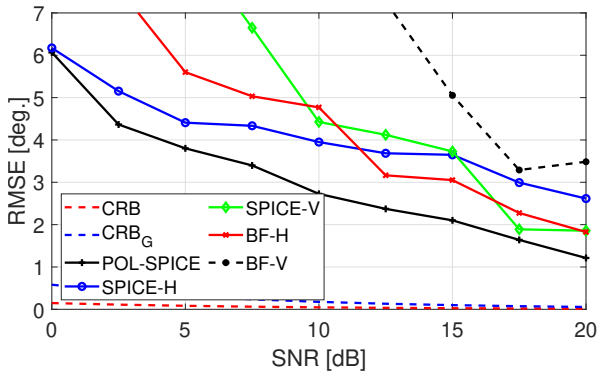

(b)

FIGURE 10: RMSE vs SNR for the radar scenario with $L = 1$. (a) SLIM-based procedures vs counterparts. (b) SPICE-based procedures vs counterparts.

polarization to better distinguish the two returns. Indeed, in H polarization, being $|\rho_H|$=0.97, the two returns (direct and multipath) have similar values, whereas in V polarization, being $|\rho_V| = 0.58$, the echo from the direct path is much stronger than the multipath one, making the actual target DOA estimation process easier. However, the POL-SPICE and POL-SLIM methods provide substantially better performance regardless of the SNR value, with a noticeable advantage of the POL-SPICE over the counterparts, corroborating again its effectiveness also in this challenging scenario characterized by a single data snapshot and two closely-located and correlated returns (direct contribution and multipath).

V. CONCLUSION

In this paper, two iterative algorithms, POL-SLIM and POL-SPICE, have been proposed for DOA estimation in a sensor array with crossed dipole receive pairs. The devised estimators can be framed as extensions of the conventional sparse methods, i.e., SLIM and SPICE, to the polarimetric domain. Toward this goal, a tailored polarimetric dictionary, composed of generalized matrix atoms (given by the polarimetric array manifolds), has been considered to model the sparse signal. Therefore, bespoke solutions to the optimization problems involved in the SLIM and SPICE-based estimation processes have been derived (also capitalizing on prior knowledge on the noise variance), which, together with the sparse model formulation, represent the main technical contributions of this paper. Hence, by leveraging the sparsity of the signal model and capitalizing on its polarimetric characteristic, POL-SLIM and POL-SPICE proved able to yield high-resolution DOA estimates. Precisely, their RMSE performance has been numerically assessed in several practical scenarios, including a typical passive sensing case and a radar operating in a multipath context. Moreover, comparison with the CRB and single-polarization counterparts available in the open literature has also been thoroughly considered. The results have clearly highlighted the effectiveness of the synthesized estimation architectures and their advantages over the counterparts.

Future developments may include the application of the devised framework to the case of different subarrays in H and V polarizations, in terms of number of elements and/or antennas characteristics, i.e., having distinct array manifold expressions. Other possible extensions may be aimed at taking into account, at the design stage, the presence of non-idealities, e.g., due to mutual coupling effects, that could lead to considerable performance loss if not adequately compensated [45] as well as off grid sources returns. Finally, it deserves further analysis the limiting DOA estimation performance using crossed-dipoles array via the Ziv-Zakai bound [46] in the polarimetric domain.

APPENDIX

A. SOLUTION TO PROBLEM IN (14)

Let us write the objective function in (14) as

$$\begin{aligned}
&\frac{\|\boldsymbol{H}\boldsymbol{X}-\boldsymbol{Y}\|_F^2}{\eta^{(n)}}+\|\boldsymbol{D}_{\bar{\boldsymbol{X}}}^{P}\boldsymbol{X}\|_F^2\\
&=\operatorname{tr}\left(\frac{(\boldsymbol{H}\boldsymbol{X}-\boldsymbol{Y})^\dagger(\boldsymbol{H}\boldsymbol{X}-\boldsymbol{Y})}{\eta^{(n)}}\right)+\operatorname{tr}\left(\boldsymbol{X}^\dagger\boldsymbol{D}_{\bar{\boldsymbol{X}}}^{P\dagger}\boldsymbol{D}_{\bar{\boldsymbol{X}}}^{P}\boldsymbol{X}\right)\\
&=\operatorname{tr}\left(\frac{\boldsymbol{X}^\dagger\boldsymbol{H}^\dagger\boldsymbol{H}\boldsymbol{X}-\boldsymbol{X}^\dagger\boldsymbol{H}^\dagger\boldsymbol{Y}-\boldsymbol{Y}^\dagger\boldsymbol{H}\boldsymbol{X}+\boldsymbol{Y}^\dagger\boldsymbol{Y}}{\eta^{(n)}}\right)\\
&\quad+\operatorname{tr}\left(\boldsymbol{X}^\dagger\boldsymbol{D}_{\bar{\boldsymbol{X}}}^{P\dagger}\boldsymbol{D}_{\bar{\boldsymbol{X}}}^{P}\boldsymbol{X}\right)\\
&=\operatorname{tr}\left(\boldsymbol{X}^\dagger\left(\frac{\boldsymbol{H}^\dagger\boldsymbol{H}}{\eta^{(n)}}+\boldsymbol{D}_{\bar{\boldsymbol{X}}}^{P\dagger}\boldsymbol{D}_{\bar{\boldsymbol{X}}}^{P}\right)\boldsymbol{X}\right)\\
&\quad-\operatorname{tr}\left(\frac{\boldsymbol{X}^\dagger\boldsymbol{H}^\dagger\boldsymbol{Y}-\boldsymbol{Y}^\dagger\boldsymbol{H}\boldsymbol{X}}{\eta^{(n)}}\right)+K_1
\end{aligned}\tag{52}$$

with K_1 functionally independent of $\boldsymbol{X}$. Now, computing and nulling the gradient of (52) w.r.t. $\boldsymbol{X}$ yields

$$\left(\frac{\boldsymbol{H}^\dagger\boldsymbol{H}}{\eta^{(n)}}+\boldsymbol{D}_{\bar{\boldsymbol{X}}}^{P\dagger}\boldsymbol{D}_{\bar{\boldsymbol{X}}}^{P}\right)\boldsymbol{X}-\frac{\boldsymbol{H}^\dagger\boldsymbol{Y}}{\eta^{(n)}}=\boldsymbol{0}.\tag{53}$$

Thus, a stationary point of (14) is given by

$$\hat{\boldsymbol{X}}=\left(\boldsymbol{H}^\dagger\boldsymbol{H}+\eta^{(n)}\boldsymbol{D}_{\bar{\boldsymbol{X}}}^{P\dagger}\boldsymbol{D}_{\bar{\boldsymbol{X}}}^{P}\right)^{-1}\boldsymbol{H}^\dagger\boldsymbol{Y}.\tag{54}$$

B. PROOF THAT FOR $L=1$ THE SPICE CRITERION (25) CAN POSSIBLY YIELD TO A ILL-POSED OPTIMIZATION PROBLEM

To begin with, let us notice that the SPICE fitting criterion (25), for the case of $L=1$, can be equivalently written as

$$\begin{aligned}
&\left\|\boldsymbol{R}^{-\frac{1}{2}}\left(\boldsymbol{R}_{SCM}-\boldsymbol{R}\right)\right\|_F^2\\
&=\operatorname{tr}\left(\left(\boldsymbol{R}_{SCM}-\boldsymbol{R}\right)\boldsymbol{R}^{-1}\left(\boldsymbol{R}_{SCM}-\boldsymbol{R}\right)\right)\\
&=\operatorname{tr}(\boldsymbol{R}_{SCM}\boldsymbol{R}^{-1}\boldsymbol{R}_{SCM})+\operatorname{tr}(\boldsymbol{R})-2\operatorname{tr}(\boldsymbol{R}_{SCM}).
\end{aligned}\tag{55}$$

In this case the sample covariance can be rewritten as $\boldsymbol{R}_{SCM}=\boldsymbol{a}\boldsymbol{a}^\dagger$, so (55) is given by

$$\begin{aligned}
&\operatorname{tr}(\boldsymbol{a}\boldsymbol{a}^\dagger\boldsymbol{R}^{-1}\boldsymbol{a}\boldsymbol{a}^\dagger)+\operatorname{tr}(\boldsymbol{R})-2\|\boldsymbol{a}\|^2\\
&=\|\boldsymbol{a}\|^2\boldsymbol{a}^\dagger\boldsymbol{R}^{-1}\boldsymbol{a}+\operatorname{tr}(\boldsymbol{R})\\
&\geq\|\boldsymbol{a}\|^4\lambda_{min}(\boldsymbol{R}^{-1})+\sum_{i=1}^{N}\lambda_i(\boldsymbol{R})\\
&=\|\boldsymbol{a}\|^4\frac{1}{\lambda_{max}(\boldsymbol{R})}+\lambda_{max}(\boldsymbol{R})+\sum_{i=2}^{N}\lambda_i(\boldsymbol{R})\\
&\geq\|\boldsymbol{a}\|^4\frac{1}{\sqrt{\|\boldsymbol{a}\|^4}}+\sqrt{\|\boldsymbol{a}\|^4}+\sum_{i=2}^{N}\lambda_i(\boldsymbol{R})\\
&\geq 2\|\boldsymbol{a}\|^2,
\end{aligned}\tag{56}$$

whereby the infimum $2\|\boldsymbol{a}\|^2$ can be only achieved when the covariance matrix is semidefinite, i.e.,

$$\boldsymbol{R}=\boldsymbol{a}\boldsymbol{a}^\dagger+\lim_{n\to\infty}\frac{1}{n}\boldsymbol{I}\succeq\boldsymbol{0},\tag{57}$$

which means that the unconstrained optimal solution lies on the boundaries of the feasible set.

C. POL-SPICE updating rules

In the following, the optimization of the objective function in (30) w.r.t. $\boldsymbol{C}$ is studied. Then, fixing $\boldsymbol{C}$, the estimates of $\boldsymbol{P}$ and η are derived.

Assuming $\boldsymbol{P}$ and η fixed parameters, by denoting $\bar{\boldsymbol{P}}=\operatorname{diag}(\boldsymbol{P},\eta\boldsymbol{I}_{2N})$, the solution for $\boldsymbol{C}$ is given by [18]

$$\hat{\boldsymbol{C}}=\bar{\boldsymbol{P}}\bar{\boldsymbol{H}}^\dagger(\bar{\boldsymbol{H}}\bar{\boldsymbol{P}}\bar{\boldsymbol{H}}^\dagger)^{-1}\tilde{\boldsymbol{R}}^{\frac{1}{2}}.\tag{58}$$

Let us now analyze the optimization problem when $\boldsymbol{C}$ is held fixed, with its value set to $\hat{\boldsymbol{C}}$. To begin with, it is worth noting that

$$\operatorname{tr}(\hat{\boldsymbol{C}}^\dagger\bar{\boldsymbol{P}}^{-1}\hat{\boldsymbol{C}})=\sum_{i=1}^{\bar{N}}\operatorname{tr}(\hat{\boldsymbol{C}}_i^\dagger\boldsymbol{P}_i^{-1}\hat{\boldsymbol{C}}_i)+\frac{1}{\eta}\sum_{i=\bar{N}+1}^{\bar{N}+N}\|\hat{\boldsymbol{C}}_i\|_F^2.\tag{59}$$

Thus, the optimization problem (30) w.r.t. $\boldsymbol{P}$ and η is tantamount to considering

$$\min_{\boldsymbol{P}\succ\boldsymbol{0},\eta>0}\ h(\boldsymbol{P},\eta)\tag{60}$$

with

$$\begin{aligned}
h(\boldsymbol{P},\eta)=&\sum_{i=1}^{\bar{N}}\operatorname{tr}(\hat{\boldsymbol{C}}_i^\dagger\boldsymbol{P}_i^{-1}\hat{\boldsymbol{C}}_i)+\frac{1}{\eta}\sum_{i=\bar{N}+1}^{\bar{N}+N}\|\hat{\boldsymbol{C}}_i\|_F^2\\
&+\sum_{i=1}^{\bar{N}}\operatorname{tr}(\boldsymbol{H}_i^\dagger\tilde{\boldsymbol{R}}^{-1}\boldsymbol{H}_i\boldsymbol{P}_i)+\eta\operatorname{tr}(\tilde{\boldsymbol{R}}^{-1})
\end{aligned}\tag{61}$$

Therefore, the optimal solution w.r.t. $\boldsymbol{P}=[\boldsymbol{P}_1,\ldots,\boldsymbol{P}_{\bar{N}}]$ is obtained as the point satisfying

$$\frac{\nabla h(\boldsymbol{P},\eta)}{\nabla\boldsymbol{P}_i}=\boldsymbol{0}\tag{62}$$

leading to the expressions

$$\hat{\boldsymbol{P}}_i^{-1}\hat{\boldsymbol{C}}_i\hat{\boldsymbol{C}}_i^\dagger\hat{\boldsymbol{P}}_i^{-1}=\boldsymbol{H}_i^\dagger\tilde{\boldsymbol{R}}^{-1}\boldsymbol{H}_i,\ i=1,\ldots,\bar{N}.\tag{63}$$

By defining $\boldsymbol{Z}_i=(\hat{\boldsymbol{C}}_i\hat{\boldsymbol{C}}_i^\dagger)^{\frac{1}{2}}$, (63) can be equivalently written as

$$\boldsymbol{Z}_i\hat{\boldsymbol{P}}_i^{-1}\boldsymbol{Z}_i\boldsymbol{Z}_i\hat{\boldsymbol{P}}_i^{-1}\boldsymbol{Z}_i=\boldsymbol{Z}_i\boldsymbol{H}_i^\dagger\tilde{\boldsymbol{R}}^{-1}\boldsymbol{H}_i\boldsymbol{Z}_i\tag{64}$$

which, by letting $\boldsymbol{Q}_i=\boldsymbol{Z}_i^{-1}\hat{\boldsymbol{P}}_i\boldsymbol{Z}_i^{-1}$, yields

$$\boldsymbol{Q}_i^{-2}=\boldsymbol{Z}_i\boldsymbol{H}_i^\dagger\tilde{\boldsymbol{R}}^{-1}\boldsymbol{H}_i\boldsymbol{Z}_i\tag{65}$$

that leads to

$$\boldsymbol{Q}_i=\boldsymbol{Z}_i^{-1}\hat{\boldsymbol{P}}_i\boldsymbol{Z}_i^{-1}=\left[\boldsymbol{Z}_i^{-1}\left(\boldsymbol{H}_i^\dagger\tilde{\boldsymbol{R}}^{-1}\boldsymbol{H}_i\right)^{-1}\boldsymbol{Z}_i^{-1}\right]^{\frac{1}{2}}.\tag{66}$$

Therefore

$$\hat{\boldsymbol{P}}_i=\boldsymbol{Z}_i\left[\boldsymbol{Z}_i^{-1}\left(\boldsymbol{H}_i^\dagger\tilde{\boldsymbol{R}}^{-1}\boldsymbol{H}_i\right)^{-1}\boldsymbol{Z}_i^{-1}\right]^{\frac{1}{2}}\boldsymbol{Z}_i,\ i=1,\ldots,\bar{N},\tag{67}$$

Finally, regarding η, it is straightforward to prove that

$$\hat{\eta}=\min\left(\max\left(\eta_L,\check{\eta}\right),\eta_U\right),\tag{68}$$

where

$$\check{\eta} = \sqrt{\frac{\sum_{i=\bar{N}+1}^{\bar{N}+N} \left\| \boldsymbol{C}_i^{(n)} \right\|_F^2}{\mathrm{tr}(\tilde{\boldsymbol{R}}^{-1})}} \tag{69}$$

is the corresponding unconstrained estimate, obtained by computing and nulling the partial derivative of the objective function in (60) w.r.t. η.

D. PROOF THAT EACH BLOCK VARIABLE OF $\mathcal{P}_2$ IS OPTIMIZED OVER A COMPACT CONVEX SET

In the following, the feasible sets, related to each block variable optimization in **Algorithm 2**, are proven to be compact convex sets. To begin with, notice that due to considered prior knowledge on the white noise power, η is bounded by lower and upper bounds, i.e., so η is optimized over $\mathbb{S}_1 = [\eta_L, \eta_U]$. Then, being $\boldsymbol{H}_i^\dagger \tilde{\boldsymbol{R}}^{-1} \boldsymbol{H}_i \succ \boldsymbol{0}$, it follows that

- $f(\boldsymbol{C}, \boldsymbol{P}, \eta)$ diverges for $\|\boldsymbol{P}_i\|_F \to \infty$, so $\exists \zeta_P \in \mathbb{R}^+$ such that the optimization of $\boldsymbol{P}_i$ can be performed focusing on the non-empty compact and convex set $\mathbb{S}_2^i = \{\|\boldsymbol{P}_i\|_F \leq \zeta_P\}, i = 1, \ldots, \bar{N}$;
- $f(\boldsymbol{C}, \boldsymbol{P}, \eta)$ diverges for $\|\boldsymbol{C}\|_F \to \infty$ being

$$f(\boldsymbol{C}, \boldsymbol{P}, \eta) \geq \mathrm{tr}(\boldsymbol{C}^\dagger \bar{\boldsymbol{P}}^{-1} \boldsymbol{C}) \geq \|\boldsymbol{C}\|_F^2 \lambda_{max}(\bar{\boldsymbol{P}}), \tag{70}$$

with $\lambda_{max}(\bar{\boldsymbol{P}}) \leq \max(\zeta_P, \eta_U)$, so $\exists \zeta_C \in \mathbb{R}^+$ such that the search space can be restricted to the non-empty compact and convex set $\mathbb{S}_3 = \{\|\boldsymbol{C}\|_F\} \leq \zeta_C$.

Therefore, the optimization process can be focused on the non-empty compact and convex set given by $\mathbb{S}_1 \times \mathbb{S}_2 \times \mathbb{S}_3$, where $\mathbb{S}_2 = \mathbb{S}_2^1 \times \mathbb{S}_2^2 \times \cdots \times \mathbb{S}_2^{\bar{N}}$.

E. CRB

Aimed at a proper understanding of the statistical efficiency of the devised signal processing strategies, in the following, the CRB for sources DOA estimation is devised, which represents a lower bound on the accuracy of any unbiased estimators [3].

1) Unknown nonrandom sources

With reference to the signal model (1), assuming the sources amplitude be unknown nonrandom complex terms, the vector whose entries are the unknown parameters is given by

$$\boldsymbol{\theta} = [\bar{\boldsymbol{\theta}}^{\mathrm{T}}, \boldsymbol{F}^{\mathrm{T}}, \eta]^{\mathrm{T}} \in \mathbb{R}^{K+4KL+1} \tag{71}$$

with

$$\bar{\boldsymbol{\theta}} = [\bar{\theta}_1, \ldots, \bar{\theta}_K]^{\mathrm{T}} \in \mathbb{R}^K \tag{72}$$

and

$$\boldsymbol{F} = [\boldsymbol{F}_1^{\mathrm{T}}, \ldots, \boldsymbol{F}_L^{\mathrm{T}}] \in \mathbb{R}^{4KL} \tag{73}$$

where, for $l = 1, \ldots, L$,

$$\boldsymbol{F}_l = \Big[\mathfrak{Re}\{\bar{x}_{1,l}^{(\mathrm{H})}\}, \mathfrak{Im}\{\bar{x}_{1,l}^{(\mathrm{H})}\}, \mathfrak{Re}\{\bar{x}_{1,l}^{(\mathrm{V})}\}, \mathfrak{Im}\{\bar{x}_{1,l}^{(\mathrm{V})}\}, \ldots, \mathfrak{Re}\{\bar{x}_{K,l}^{(\mathrm{H})}\}, \mathfrak{Im}\{\bar{x}_{K,l}^{(\mathrm{H})}\}, \mathfrak{Re}\{\bar{x}_{K,l}^{(\mathrm{V})}\}, \mathfrak{Im}\{\bar{x}_{K,l}^{(\mathrm{V})}\}\Big]^{\mathrm{T}} \in \mathbb{R}^{4K}. \tag{74}$$

Therefore, the CRB on $\bar{\boldsymbol{\theta}}$ is [3]

$$\mathrm{CRB}_{\boldsymbol{\theta}} = \left(\frac{2}{\eta} \sum_{l=1}^{L} \mathfrak{Re}\{\boldsymbol{Z}_l^\dagger \boldsymbol{D}^\dagger \boldsymbol{P}_S^o \boldsymbol{D} \boldsymbol{Z}_l\} \right)^{-1} \tag{75}$$

where

$$\boldsymbol{Z}_l = \mathrm{diag}(\bar{\boldsymbol{x}}_{1,l}, \bar{\boldsymbol{x}}_{2,l}, \ldots, \bar{\boldsymbol{x}}_{K,l}) \in \mathbb{C}^{2K \times K} \tag{76}$$

$$\boldsymbol{D} = [\dot{\boldsymbol{S}}(\bar{\theta}_1), \dot{\boldsymbol{S}}(\bar{\theta}_2), \ldots, \dot{\boldsymbol{S}}(\bar{\theta}_K)] \in \mathbb{C}^{2N \times 2K} \tag{77}$$

$$\boldsymbol{P}_S^o = \boldsymbol{I} - \boldsymbol{P}_S \in \mathbb{C}^{2N \times 2N} \tag{78}$$

with

$$\boldsymbol{P}_S = \tilde{\boldsymbol{S}} \left(\tilde{\boldsymbol{S}}^\dagger \tilde{\boldsymbol{S}} \right)^{-1} \tilde{\boldsymbol{S}}^\dagger \in \mathbb{C}^{2N \times 2N} \tag{79}$$

$$\tilde{\boldsymbol{S}} = \left[\boldsymbol{S}(\bar{\theta}_1), \boldsymbol{S}(\bar{\theta}_2), \ldots, \boldsymbol{S}(\bar{\theta}_K) \right] \in \mathbb{C}^{2N \times 2K} \tag{80}$$

while

$$\dot{\boldsymbol{S}}(\bar{\theta}_m) = \begin{bmatrix} \dot{\boldsymbol{s}}(\bar{\theta}_m) & \boldsymbol{0} \\ \boldsymbol{0} & \dot{\boldsymbol{s}}(\bar{\theta}_m) \end{bmatrix} = \boldsymbol{I}_2 \otimes \dot{\boldsymbol{s}}(\bar{\theta}_m) \in \mathbb{C}^{2N \times 2} \tag{81}$$

with $\dot{\boldsymbol{s}}(\bar{\theta}_m) = \frac{\partial \boldsymbol{s}(\bar{\theta}_m)}{\partial \theta_m}$, which, for a ULA, becomes

$$\dot{\boldsymbol{s}}(\bar{\theta}_m) = \boldsymbol{s}(\bar{\theta}_m) \odot [0, j\pi, \ldots, j\pi(N-1)]^{\mathrm{T}}. \tag{82}$$

Finally, the mean CRB on DOA estimation (averaging (75) over the number of sources) is computed as

$$\mathrm{CRB} = \frac{1}{K} \mathrm{tr}\left(\mathrm{CRB}_{\boldsymbol{\theta}}\right). \tag{83}$$

2) Unknown Gaussian sources

Under the assumption of Gaussian sources, the unknown spectral matrix is

$$\tilde{\boldsymbol{R}} = \sum_{m=1}^{K} \boldsymbol{S}(\bar{\theta}_m) \tilde{\boldsymbol{P}}_i \boldsymbol{S}(\bar{\theta}_m) + \eta \boldsymbol{I} = \tilde{\boldsymbol{S}} \tilde{\boldsymbol{P}} \tilde{\boldsymbol{S}}^\dagger + \eta \boldsymbol{I}_{2N} \tag{84}$$

where $\tilde{\boldsymbol{S}} = [\boldsymbol{S}(\bar{\theta}_1), \ldots, \boldsymbol{S}(\bar{\theta}_K)] \in \mathbb{C}^{2N \times 2K}$ and $\tilde{\boldsymbol{P}} = \mathrm{diag}([\tilde{\boldsymbol{P}}_1, \ldots, \tilde{\boldsymbol{P}}_K]) \in \mathbb{R}^{2K \times 2K}$ with $\tilde{\boldsymbol{P}}_i = \begin{bmatrix} P_{i,H} & P_{i,HV} \\ P_{i,HV} & P_{i,V} \end{bmatrix} = \mathbb{E}[\bar{\boldsymbol{x}}_{m,1} \bar{\boldsymbol{x}}_{m,1}^\dagger] = \cdots = \mathbb{E}[\bar{\boldsymbol{x}}_{m,L} \bar{\boldsymbol{x}}_{m,L}^\dagger] \in \mathbb{R}^{2 \times 2}$ the polarimetric covariance matrix of the i-th source. Therefore, with reference to (84), the unknown vector of parameters is

$$\boldsymbol{\theta} = [\bar{\boldsymbol{\theta}}^{\mathrm{T}}, \bar{\boldsymbol{P}}^{\mathrm{T}}, \eta]^{\mathrm{T}} \in \mathbb{R}^{4K+1} \tag{85}$$

with

$$\bar{\boldsymbol{\theta}} = [\bar{\theta}_1, \ldots, \bar{\theta}_K]^{\mathrm{T}} \in \mathbb{R}^K \tag{86}$$

and

$$\bar{\boldsymbol{P}} = [P_{1,H}, P_{1,HV}, P_{1,V}, P_{2,H}, P_{2,HV}, P_{2,V}, \ldots, P_{K,H}, P_{K,HV}, P_{K,V}] \in \mathbb{R}^{3K}. \tag{87}$$

Under this scenario, the mean CRB on DOA estimation is computed as

$$\text{CRB} = \frac{1}{K}\,\text{tr}\left(\text{CRB}_{\boldsymbol{\theta},G}\right) \tag{88}$$

where the CRB for $\bar{\boldsymbol{\theta}}$ estimation is given by [3]

$$\text{CRB}_{\boldsymbol{\theta},G} = \frac{\eta}{2L}\left(\mathfrak{Re}\{[\tilde{\boldsymbol{P}}\tilde{\boldsymbol{S}}^{\dagger}\tilde{\boldsymbol{R}}^{-1}\tilde{\boldsymbol{S}}\tilde{\boldsymbol{P}}] \odot [\tilde{\boldsymbol{D}}^{\dagger}\boldsymbol{P}_{\tilde{S}}^{\perp}\tilde{\boldsymbol{D}}]^{\mathrm{T}}\}\right)^{-1} \tag{89}$$

with

$$\tilde{\boldsymbol{D}} = [\dot{\boldsymbol{S}}(\bar{\theta}_1), \ldots, \dot{\boldsymbol{S}}(\bar{\theta}_K)] \in \mathbb{C}^{2N\times 2K} \tag{90}$$

and

$$\boldsymbol{P}_{\tilde{S}}^{\perp} = \boldsymbol{I}_{2N} - \tilde{\boldsymbol{S}}\left(\tilde{\boldsymbol{S}}^{\dagger}\tilde{\boldsymbol{S}}\right)^{-1}\tilde{\boldsymbol{S}}^{\dagger} \in \mathbb{C}^{2N\times 2N} \tag{91}$$

F. Implementation of Polarimetric MUSIC

This subsection describes the implementation of a polarimetric version of the MUSIC algorithm.

1) Compute the sample covariance matrix $\boldsymbol{R}_{SCM} = \frac{1}{L}\boldsymbol{Y}\boldsymbol{Y}^{\dagger}$;
2) Perform the eigendecomposition of $\boldsymbol{R}_{SCM}$ as
$$\boldsymbol{R}_{SCM} = \boldsymbol{U}\boldsymbol{\Lambda}\boldsymbol{U}^{H}, \tag{92}$$
where $\boldsymbol{\Lambda}$ is the diagonal matrix of eigenvalues arranged in descending order and $\boldsymbol{U}$ is the matrix of the corresponding eigenvectors;
3) Partition $\boldsymbol{U}$ as
$$\boldsymbol{U} = \begin{bmatrix}\boldsymbol{U}_{\text{signal}} & \boldsymbol{U}_{\text{noise}}\end{bmatrix}, \tag{93}$$
where $\boldsymbol{U}_{\text{signal}}$ contains the eigenvectors corresponding to the $2K$ largest eigenvalues (assuming K sources), and $\boldsymbol{U}_{\text{noise}}$ contains the remaining $2(N-K)$ eigenvectors spanning the noise subspace;
4) Evaluate the polarimetric spatial power spectrum for the angle θ_i as
$$\text{SPS}(\theta_i) = \frac{1}{\|\boldsymbol{U}_{\text{noise}}^{\dagger}\boldsymbol{H}_i\|_F^2}; \tag{94}$$
5) Estimate the DOAs as the angles θ_i corresponding to the K highest peaks in the SPS.

REFERENCES

[1] M. A. Richards, J. A. Scheer, and W. A. Holm, *Principles of Modern Radar: Basic Principles*, ser. Radar, Sonar & Navigation. Stevenage, U.K.: Institution of Engineering and Technology, 2010.

[2] M. A. Ainslie, *Principles of sonar performance modelling*. Berlin: Springer, 2010.

[3] H. L. V. Trees, *Optimum Array Processing: Part IV, Detection, Estimation, and Modulation Theory*. Hoboken, NJ, USA: Wiley, 2004.

[4] B. Friedlander, "Antenna array manifolds for high-resolution direction finding," *IEEE Trans. Signal Process.*, vol. 66, no. 4, pp. 923–932, Feb. 2018.

[5] R. Roy and T. Kailath, "ESPRIT-estimation of signal parameters via rotational invariance techniques," *IEEE Trans. on Acoustics, Speech, and Signal Process.*, vol. 37, no. 7, pp. 984–995, 1989.

[6] J. Capon, "High-resolution frequency-wavenumber spectrum analysis," *Proceedings of the IEEE*, vol. 57, no. 8, pp. 1408–1418, 1969.

[7] B. Ottersten, M. Viberg, and T. Kailath, "Performance analysis of the total least squares ESPRIT algorithm," *IEEE Transactions on Signal Processing*, vol. 39, no. 5, pp. 1122–1135, 1991.

[8] R. Schmidt, "Multiple emitter location and signal parameter estimation," *IEEE Transactions on Antennas and Propagation*, vol. 34, no. 3, pp. 276–280, 1986.

[9] R. A. Poisel, *Introduction to communication electronic warfare systems*. Artech House, Inc., 2008.

[10] P.-J. Chung, M. Viberg, and J. Yu, "DOA estimation methods and algorithms," in *Academic Press Library in Signal Processing*. Elsevier, 2014, vol. 3, pp. 599–650.

[11] H. Krim and M. Viberg, "Two decades of array signal processing research: the parametric approach," *IEEE Signal Processing Magazine*, vol. 13, no. 4, pp. 67–94, 1996.

[12] P. Stoica and A. Nehorai, "On the concentrated stochastic likelihood function in array signal processing," *Circuits, Systems and Signal Processing*, vol. 14, no. 5, pp. 669–674, 1995.

[13] ——, "Performance study of conditional and unconditional direction-of-arrival estimation," *IEEE Transactions on Acoustics, Speech, and Signal Processing*, vol. 38, no. 10, pp. 1783–1795, 1990.

[14] Y. Bresler and A. Macovski, "Exact maximum likelihood parameter estimation of superimposed exponential signals in noise," *IEEE Transactions on Acoustics, Speech, and Signal Processing*, vol. 34, no. 5, pp. 1081–1089, 1986.

[15] P. Stoica and K. C. Sharman, "Novel eigenanalysis method for direction estimation," in *IEE Proceedings F (Radar and Signal Processing)*, vol. 137, no. 1. IET, 1990, pp. 19–26.

[16] S. Cotter, B. Rao, K. Engan, and K. Kreutz-Delgado, "Sparse solutions to linear inverse problems with multiple measurement vectors," *IEEE Transactions on Signal Processing*, vol. 53, no. 7, pp. 2477–2488, 2005.

[17] E. van den Berg and M. P. Friedlander, "Sparse optimization with least-squares constraints," *SIAM J. Optimization*, vol. 21, no. 4, pp. 1201–1229, 2011.

[18] Z. Yang, J. Li, P. Stoica, and L. Xie, "Chapter 11 - sparse methods for direction-of-arrival estimation," in *Academic Press Library in Signal Processing, Volume 7*, R. Chellappa and S. Theodoridis, Eds. Academic Press, 2018, pp. 509–581.

[19] X. Tan, W. Roberts, J. Li, and P. Stoica, "Sparse learning via iterative minimization with application to MIMO radar imaging," *IEEE Transactions on Signal Processing*, vol. 59, no. 3, pp. 1088–1101, 2011.

[20] A. Aubry, V. Carotenuto, A. De Maio, and M. A. Govoni, "Multi-snapshot spectrum sensing for cognitive radar via block-sparsity exploitation," *IEEE Transactions on Signal Processing*, vol. 67, no. 6, pp. 1396–1406, 2019.

[21] P. Stoica, P. Babu, and J. Li, "SPICE: A sparse covariance-based estimation method for array processing," *IEEE Transactions on Signal Processing*, vol. 59, no. 2, pp. 629–638, 2011.

[22] P. Stoica, D. Zachariah, and J. Li, "Weighted SPICE: A unifying approach for hyperparameter-free sparse estimation," *Digital Signal Processing*, vol. 33, pp. 1–12, 2014.

[23] J. Li and R. T. Compton, "Angle and polarization estimation using ESPRIT with a polarization sensitive array," *IEEE Trans. on Antennas Propag.*, vol. 39, no. 9, pp. 1376–1383, 1991.

[24] B. K. Chalise, Y. D. Zhang, and B. Himed, "Compressed sensing based joint DOA and polarization angle estimation for sparse arrays with dual-polarized antennas," in *IEEE GlobalSIP 2018*, 2018, pp. 251–255.

[25] E. Ferrara and T. Parks, "Direction finding with an array of antennas having diverse polarizations," *IEEE Transactions on Antennas and Propagation*, vol. 31, no. 2, pp. 231–236, 1983.

[26] S. Qiu, W. Sheng, X. Ma, and T. Kirubarajan, "A maximum likelihood method for joint DOA and polarization estimation based on manifold separation," *IEEE Transactions on Aerospace and Electronic Systems*, vol. 57, no. 4, pp. 2481–2500, 2021.

[27] Wong, L. Li, and Zoltowski, "Root-MUSIC-based direction-finding and polarization estimation using diversely polarized possibly collocated antennas," *IEEE Antennas and Wireless Propagation Letters*, vol. 3, pp. 129–132, 2004.

[28] J. Li and R. Compton, "Angle estimation using a polarization sensitive array," *IEEE Transactions on Antennas and Propagation*, vol. 39, no. 10, pp. 1539–1543, 1991.

[29] A. Weiss and B. Friedlander, "Performance analysis of diversely polarized antenna arrays," *IEEE Transactions on Signal Processing*, vol. 39, no. 7, pp. 1589–1603, 1991.

[30] A. Aubry, A. De Maio, and A. Farina, Eds., *Polarimetric Radar Signal Processing*, ser. Radar, Sonar and Navigation. Stevenage, England: Institution of Engineering and Technology, 2022.
[31] M. Rosamilia, M. Boddi, A. Aubry, and A. De Maio, "Polarimetric sparse iterative procedures for DOA estimation," in *2023 IEEE International Workshop on Technologies for Defense and Security (TechDefense), Rome, Italy*. IEEE, 19 Nov. 2023.
[32] D. R. Hunter and K. Lange, "A tutorial on MM algorithms," *The American Statistician*, vol. 58, no. 1, pp. 30–37, 2004.
[33] M. Razaviyayn, M. Hong, and Z.-Q. Luo, "A unified convergence analysis of block successive minimization methods for nonsmooth optimization," *SIAM Journal on Optimization*, vol. 23, no. 2, pp. 1126–1153, 2013.
[34] Y. Sun, P. Babu, and D. P. Palomar, "Majorization-minimization algorithms in signal processing, communications, and machine learning," *IEEE Trans. Signal Process.*, vol. 65, no. 3, pp. 794–816, 2016.
[35] A. Aubry, V. Carotenuto, A. De Maio, M. A. Govoni, and A. Farina, "Experimental analysis of block-sparsity-based spectrum sensing techniques for cognitive radar," *IEEE Transactions on Aerospace and Electronic Systems*, vol. 57, no. 1, pp. 355–370, 2021.
[36] D. Malioutov, M. Cetin, and A. Willsky, "A sparse signal reconstruction perspective for source localization with sensor arrays," *IEEE Transactions on Signal Processing*, vol. 53, no. 8, pp. 3010–3022, 2005.
[37] M. S. Lobo, L. Vandenberghe, S. Boyd, and H. Lebret, "Applications of second-order cone programming," *Linear algebra and its applications*, vol. 284, no. 1-3, pp. 193–228, 1998.
[38] M. Steiner and K. Gerlach, "Fast converging adaptive processor or a structured covariance matrix," *IEEE Transactions on Aerospace and Electronic Systems*, vol. 36, no. 4, pp. 1115–1126, 2000.
[39] A. Aubry, A. De Maio, S. Marano, and M. Rosamilia, "Structured covariance matrix estimation with missing-(complex) data for radar applications via expectation-maximization," *IEEE Transactions on Signal Processing*, vol. 69, pp. 5920–5934, 2021.
[40] A. Aubry, A. De Maio, and V. Carotenuto, "Optimality claims for the FML covariance estimator with respect to two matrix norms," *IEEE Transactions on Aerospace and Electronic Systems*, vol. 49, no. 3, pp. 2055–2057, 2013.
[41] Y. Nesterov, "Introductory lectures on convex optimization: A basic course," *Springer Science & Business Media*, vol. 87, 2003.
[42] D. P. Bertsekas, "Nonlinear programming," *Journal of the Operational Research Society*, vol. 48, no. 3, pp. 334–334, 1997.
[43] J. Wu, *Advanced Metric Wave Radar*. Springer, 2020.
[44] L. Novak, M. Sechtin, and M. Cardullo, "Studies of target detection algorithms that use polarimetric radar data," *IEEE Transactions on Aerospace and Electronic Systems*, vol. 25, no. 2, pp. 150–165, 1989.
[45] A. Aubry, A. De Maio, L. Lan, and M. Rosamilia, "Adaptive radar detection and bearing estimation in the presence of unknown mutual coupling," *IEEE Transactions on Signal Processing*, vol. 71, pp. 1248–1262, 2023.
[46] Z. Zhang, Z. Shi, and Y. Gu, "Ziv-zakai bound for DOAs estimation," *IEEE Transactions on Signal Processing*, vol. 71, pp. 136–149, 2023.